OCCAM

OXFORD CENTRE FOR COLLABORATIVE APPLIED MATHEMATICS

Thermoviscous Coating and Rimming Flow

by

G. A. Leslie
S. K. Wilson
B.R. Duffy

OCCAM Preprint Number 12/55

THERMOVISCOUS COATING AND RIMMING FLOW

by G. A. LESLIE, S. K. WILSON[‡] *and* B. R. DUFFY

(*Department of Mathematics and Statistics, University of Strathclyde, 26 Richmond Street, Glasgow G1 1XH, United Kingdom*)

[Received 19th June 2012]

Summary

A comprehensive description is obtained of steady thermoviscous (i.e. with temperature-dependent viscosity) coating and rimming flow on a uniformly rotating horizontal cylinder which is uniformly hotter or colder than the surrounding atmosphere. It is found that, as in the corresponding isothermal problem, there is a critical solution with a corresponding critical load (which depends, in general, on both the Biot number B and the thermoviscosity number V) above which no "full-film" solutions corresponding to a continuous film of fluid covering the entire outside or inside of the cylinder exist. The effect of thermoviscosity on both the critical solution and the full-film solution with a prescribed load is described. In particular, there are no full-film solutions with a prescribed load M for any value of B when $M \geq \hat{f}^{-1/2} M_{\mathrm{c}0}$ for positive V and when $M > M_{\mathrm{c}0}$ for negative V, where $\hat{f}$ is a monotonically decreasing function of V and $M_{\mathrm{c}0} \simeq 4.44272$ is the critical load in the constant-viscosity case. It is also found that when the prescribed load satisfies $M < 1.50315$ there is a narrow region of the B–V parameter plane in which backflow occurs.

1. Introduction

The influence of thermoviscosity (i.e. temperature-dependent viscosity) effects on the two-dimensional flow of a thin film of viscous fluid on either the outside (often called "coating flow") or the inside (often called "rimming flow") of a uniformly rotating horizontal cylinder is studied. The corresponding isothermal problem has been studied extensively, largely building on the pioneering work of Pukhnachev[†] (**36**) and Moffatt (**28**). Pukhnachev (**36**) discussed the existence and uniqueness of solutions for coating flow of the steady two-dimensional Navier–Stokes equations and then used lubrication theory to derive an evolution equation that includes the effects of gravity, viscosity and surface tension, while Moffatt (**28**) considered coating flow both theoretically using a model based on lubrication theory and experimentally and, in particular, found that steady continuous, finite and non-zero solutions to his model (hereafter referred to as "full-film" solutions) are possible only below a critical load.

There have been many subsequent studies of isothermal coating flow, including those by Hansen and Kelmanson (**17**) who obtained steady numerical solutions to the Stokes equations, and Duffy and Wilson (**10**) who extended Moffatt's work to include "curtain"

[‡] Author for correspondence. Presently also a Visiting Fellow in the Oxford Centre for Collaborative Applied Mathematics (OCCAM), University of Oxford, Mathematical Institute, 24–29 St. Giles', Oxford OX1 3LB. Email: s.k.wilson@strath.ac.uk

[†] This author's name has been transliterated into English as both "Pukhnachev" and "Pukhnachov".

solutions, that is, solutions that are unbounded at the top and bottom of the cylinder representing fluid falling onto and off the cylinder. Peterson, Jimack and Kelmanson (**34**) obtained unsteady numerical solutions to the Stokes equations and found that steady-state solutions are more readily attained for near-critical loads than for significantly sub-critical loads, while Wilson, Hunt and Duffy (**48**) obtained steady numerical solutions to the Stokes equations for both coating and rimming flow in the critical state and developed higher order asymptotic solutions in the limit of small aspect ratio of the film. Hinch and Kelmanson (**18**) analysed and numerically solved the evolution equation derived by Pukhnachev (**36**) and found that perturbations to the solutions decay slowly to the steady state and exhibit a phase lag, while Karabut (**25**) investigated the same model and obtained solutions representing a hanging drop, and Kelmanson (**26**) extended the work of Pukhnachev (**36**) by including inertial effects in the model. Evans, Schwartz and Roy (**13**) derived a three-dimensional evolution equation for coating flow which includes the effects of rotation, gravity and surface tension, and developed a two-dimensional numerical method for the case when axial flow is neglected. Later the same authors (**14**) extended this work to obtain numerical solutions of the three-dimensional problem and gave experimental results that confirmed the general features of the numerical simulation. Noakes, King and Riley (**29**) investigated the three-dimensional stability of coating flow in the absence of gravity, and later the same authors (**30**) considered three-dimensional rimming and coating flows in which inertial effects (including centrifugal effects) are significant, along with the effects of viscous, gravitational and surface-tension forces. Hunt (**20**) obtained unsteady numerical solutions to the Stokes equations for flow on an elliptical (rather than a circular) cylinder, and Tougher, Wilson and Duffy (**42**) analysed the approach to the critical solution found by Moffatt (**28**) valid for both rimming and coating flow.

There has also been considerable work on isothermal rimming flow. Unlike coating flow, where it is possible for fluid to drop off the cylinder if the load is too large, in rimming flow the fluid is trapped within the cylinder and so a "pool" of fluid may form within the cylinder. Johnson (**23**) considered steady rimming flow and found four types of solution, with very different free-surface profiles, two in which the fluid fully coats the cylinder, one in which the fluid pools at the bottom, and one in which the fluid coats only one side of the cylinder. Two of these profiles involve non-symmetrical solutions with a shock-like jump in the film thickness (often called "shock solutions") and have loads greater than the critical load found by Moffatt (**28**). Wilson and Williams (**45**) derived and numerically solved an evolution equation including the smoothing effect of surface tension that determines the size and location of the shock, while O'Brien and Gath (**32**) used lubrication theory to determine the height and location of the shocks without surface-tension smoothing. Tirumkudulu and Acrivos (**41**) extended the lubrication-theory model derived by Moffatt (**28**) by adding a higher-order term arising from the hydrostatic pressure, and found good agreement with experimental measurements and numerical solutions of the Stokes equations, while Acrivos and Jin (**1**) investigated the stability of the model, and the same authors (**22**) made use of the model to study three-dimensional rimming flows with axially varying viscosity. O'Brien (**31**) extended the two-dimensional lubrication-theory model by including higher-order terms arising from the hydrostatic pressure and surface tension and investigated the stability of both smooth and shock solutions. Subsequently, various aspects of the stability of the flow were examined in three papers by Benilov, O'Brien and co-workers (**4**, **5**, **6**), the latter of which considered the effect of inertia and found that while it always causes

instability, this instability may be counteracted by an increase in viscosity so as to make the time of growth so large that the solution is effectively stable. Ashmore, Hosoi and Stone (**2**) considered steady two-dimensional rimming flow where gravitational forces are large compared to viscous forces and surface-tension effects are included, resulting in a flow with a pool of fluid at the bottom of the cylinder, while Benilov, Benilov and Kopteva (**7**) investigated this pooling behaviour and derived a matched asymptotic solution describing the pool. Villegas-Díaz, Power and Riley (**44**) considered two-dimensional flow subject to a surface shear and includes the effects of surface tension and higher order gravity effects, while recently Pougatch and Frigaard (**35**) analysed a three-dimensional evolution equation that retains the terms at first order in the film aspect ratio and so included the effect of inertia as well as higher order effects of gravity and viscosity. Thoroddsen and Mahadevan (**40**) conducted an experimental study of rimming flow and described many different phenomena including a shark's-teeth-like pattern in the axial direction, while Hosoi and Mahadevan (**19**) derived an evolution equation including weak surface tension and weak inertia effects and found solutions showing the shark's-teeth pattern, and Chen, Tsai, Liu and Wu (**9**) carried out an experimental investigation into the conditions in which a uniform film occurs.

Owing to the wide range of practical situations in which thermoviscosity effects are significant there have been a number of studies of the effects of thermoviscosity on the non-isothermal flow of thin films of fluid on a variety of substrates. Thermoviscous flow of a thin film of fluid down an inclined substrate has been studied by, among others, Goussis and Kelly (**15**, **16**) and Hwang and Weng (**21**) who considered the stability of the film, Kabova and Kuznetsov (**24**) who calculated the steady flow of the film with both thermoviscous and thermocapillary (i.e. temperature-dependent surface tension) effects, and Duffy and Wilson (**11**, **46**, **47**) who studied the steady flow of a thin rivulet of fluid for three viscosity models (namely a linear, an exponential and an Eyring model). There have also been many studies of thermoviscous flow of a thin film of fluid on a horizontal substrate: Reisfeld and Bankoff (**37**) and Wu and Hwang (**50**) independently considered the evolution and eventual rupture of the film subject to surface tension and van der Waals forces, Selak and Lebon (**39**) investigated the onset of convection in a quiescent film subject to both buoyancy and thermocapillary effects, and Sansom, King and Riley (**38**) considered the spreading of the film for three viscosity models (namely a linear, an exponential and a biviscosity model). Motivated by lava flows, Bercovici (**8**) and Balmforth and Craster (**3**) studied the radial spreading of a film, with the former including thermal advection and the latter considering a viscoplastic fluid with a yield stress, while Osiptsov (**33**) considered the thermoviscous flow of a thin film of fluid over a conical surface with fluid being supplied at the apex. Unsteady flow of a thin film of fluid with thermoviscous and thermocapillary effects on a uniformly rotating disk was considered independently by Usha, Ravindran and Uma (**43**) and Wu (**49**). However, relatively little work has been done on thermoviscous coating and rimming flow on a heated or cooled horizontal cylinder. Duffy and Wilson (**12**) used lubrication theory to study steady flow on both a stationary and a uniformly rotating cylinder in the rather special case in which the free surface is at the same uniform temperature as the surrounding atmosphere and found that the film thickness (and hence the load, but not the temperature or the velocity) can be obtained by a simple re-scaling of the isothermal solution, and recently Leslie, Wilson and Duffy (**27**) analysed steady thermoviscous flow with prescribed flux on a stationary cylinder. In the present work we obtain a comprehensive description of steady thermoviscous coating and rimming flow on

a uniformly rotating horizontal cylinder. In particular, the effect of thermoviscosity on both the critical solution and the full-film solution with a prescribed load is described. In the Appendix a distinguished limit corresponding to strong thermoviscosity and weak heat transfer at the free surface in which thermoviscosity effects still enter the problem at leading order is discussed.

2. Problem Formulation

Consider the steady two-dimensional thermoviscous flow of a thin film of a Newtonian fluid with uniform density ρ and temperature-dependent viscosity $\mu = \mu(T)$, where T denotes the (in general) non-uniform temperature of the fluid, on either the outside ("coating flow") or the inside ("rimming flow") of a circular cylinder of radius a rotating in a counter-clockwise direction about its horizontal axis at uniform angular speed Ω (so that the circumferential speed is $a\Omega$), the cylinder being at the uniform temperature T_0, which may be either hotter or colder than the uniform temperature of the surrounding atmosphere, denoted by T_∞ ($\neq T_0$). Where possible we will consider a general viscosity model $\mu = \mu(T)$, where $\mu(T)$ is any monotonically decreasing function of T satisfying $\mu = \mu_0$ and $\mathrm{d}\mu/\mathrm{d}T = -\lambda\,(< 0)$ when $T = T_0$, where $\lambda\,(> 0)$ is a prescribed positive constant, and so the appropriate non-dimensional measure of thermoviscosity is the *thermoviscosity number*, V, defined by

$$V = \frac{\lambda(T_0 - T_\infty)}{\mu_0}. \tag{2.1}$$

Since V has the same sign as $T_0 - T_\infty$, situations in which the cylinder is hotter (colder) than the atmosphere correspond to positive (negative) values of V. When it is necessary to specify a particular viscosity model we will use the exponential viscosity model

$$\mu(T) = \mu_0 \exp\left(-\frac{\lambda(T - T_0)}{\mu_0}\right) \tag{2.2}$$

as used by many previous authors, for example (**3**, **15**, **16**, **21**, **27**, **39**, **46**). As, for example, Leslie, Wilson and Duffy (**27**) describe, physically realistic values of V vary over several orders of magnitude from arbitrarily small values (when the viscosity is effectively independent of temperature and/or when the magnitude of the heating or cooling is small) to reasonably large values (when the viscosity is strongly dependent on temperature and/or when the magnitude of the heating or cooling is large).

Referred to polar coordinates $r = a \pm Y$ (with origin at the cylinder's axis) and θ (measured counter-clockwise from the horizontal), as shown in Figure 1 (drawn for coating flow), we take the free surface of the fluid to be at $r = a+h$ for coating flow and $r = a-h$ for rimming flow, the film thickness being denoted by $h = h(\theta)$. The fluid velocity $\mathbf{u} = u\mathbf{e}_\theta + v\mathbf{e}_r$ (where $\mathbf{e}_\theta$ and $\mathbf{e}_r$ denote unit vectors in the azimuthal and radial directions, respectively), the pressure p, and the temperature T are governed by the usual mass-conservation, Navier–Stokes and energy equations. On the cylinder $r = a$ the velocity $\mathbf{u}$ satisfies no-slip and no-penetration conditions, and the temperature is $T = T_0$ (a prescribed constant). On the free surface $r = a \pm h$ the usual normal and tangential stress balances and the kinematic condition apply, as does Newton's law of cooling $-k_{\mathrm{th}}\nabla T \cdot \mathbf{n} = \alpha_{\mathrm{th}}(T - T_\infty)$, where k_{th} denotes the thermal conductivity of the fluid (assumed constant), $\alpha_{\mathrm{th}}\,(\geq 0)$ denotes an (empirical) surface heat-transfer coefficient, and $\mathbf{n}$ denotes the unit outward normal to

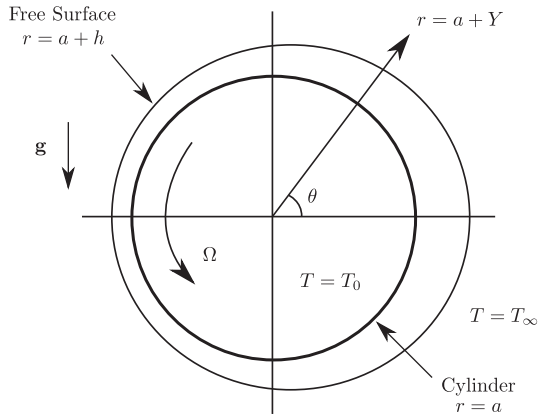

Fig. 1 Geometry of the problem (drawn for coating flow): steady two-dimensional thermoviscous flow of a thin film of Newtonian fluid on a uniformly rotating horizontal cylinder which is uniformly hotter or colder than the surrounding atmosphere.

the free surface. Surface tension, viscous dissipation, inertia and thermal advection are all neglected (which is valid provided that the appropriate capillary number is sufficiently large and that the appropriate Brinkman, Reynolds and Péclet numbers are sufficiently small).

We consider only thin films with small aspect ratio ϵ defined by

$$\epsilon = \left(\frac{\mu_0 \Omega}{\rho g a}\right)^{1/2} \ll 1, \tag{2.3}$$

where g denotes the magnitude of gravitational acceleration, and non-dimensionalise and scale the system appropriately by writing

$$\begin{gathered} r = a(1 \pm \epsilon Y^*), \quad h = \epsilon a h^*, \quad u = a\Omega u^*, \quad v = \pm \epsilon a \Omega v^*, \\ \psi = \pm \epsilon a^2 \Omega \psi^*, \quad p = p_\mathrm{a} \pm \epsilon a \rho g p^*, \quad T = T_\infty + (T_0 - T_\infty) T^*, \\ \mu = \mu_0 \mu^*, \quad Q = \epsilon a^2 \Omega Q^*, \quad M = \epsilon a^2 \rho M^*, \end{gathered} \tag{2.4}$$

in which the $+$ in the $\pm$ corresponds to coating flow while the $-$ corresponds to rimming flow, ψ is the streamfunction satisfying $u = \partial\psi/\partial Y$ and $v = -\partial\psi/\partial\theta$ with $\psi = 0$ on $Y = 0$, p_a is the constant pressure in the surrounding atmosphere, Q is the constant azimuthal volume flux of fluid per unit axial length crossing a station $\theta =$ constant, and $M\ (> 0)$ is the constant fluid load on/in the cylinder (that is, the mass of fluid per unit length on/in the cylinder). Note that since the non-dimensionalisation of temperature given in (2.4) incorporates the factor $T_0 - T_\infty$, which can be either positive or negative, care is required when interpreting results for the non-dimensional temperature T^* in terms of the dimensional temperature T. For clarity the star superscripts on non-dimensional variables will be omitted henceforth. In terms of non-dimensional variables the fluid occupies $0 \le Y \le h$ for $-\pi < \theta \le \pi$, the general viscosity model $\mu = \mu(T)$ satisfies $\mu = 1$ and $\mathrm{d}\mu/\mathrm{d}T = -V$ when $T = 1$, and the exponential viscosity model (2.2) is given by

$$\mu = \exp(-V(T-1)). \tag{2.5}$$

For both coating and rimming flow at leading order in ϵ the governing equations become

$$\frac{\partial u}{\partial \theta}+\frac{\partial v}{\partial Y}=0, \quad \frac{\partial}{\partial Y}\left(\mu\frac{\partial u}{\partial Y}\right)=\cos\theta, \quad \frac{\partial p}{\partial Y}=-\sin\theta, \quad \frac{\partial^2 T}{\partial Y^2}=0, \tag{2.6}$$

together with the boundary conditions

$$u=1, \quad v=0 \quad \text{and} \quad T=1 \quad \text{on} \quad Y=0 \tag{2.7}$$

and

$$\frac{\partial u}{\partial Y}=0, \quad p=0 \quad \text{and} \quad \frac{\partial T}{\partial Y}+BT=0 \quad \text{on} \quad Y=h, \tag{2.8}$$

where the Biot number, $B\,(\geq 0)$, defined by

$$B=\frac{\epsilon a \alpha_{\mathrm{th}}}{k_{\mathrm{th}}}, \tag{2.9}$$

is the appropriate non-dimensional measure of heat transfer to or from the atmosphere at the free surface. The special case $B=0$ corresponds to a perfectly insulated free surface with no heat transfer to or from the atmosphere (i.e. $\partial T/\partial Y=0$ on $Y=h$), while at leading order in the limit $B\to\infty$ the free surface is at the same uniform temperature as the atmosphere (i.e. $T=0$ on $Y=h$).

Introducing the rescaled radial coordinate $y=Y/h$ (so that the fluid lies within the fixed range $0\leq y\leq 1$) and solving (2.6) subject to (2.7) and (2.8) for the azimuthal velocity $u=u(y,\theta)$, the streamfunction $\psi=\psi(y,\theta)$[†], the pressure $p=p(y,\theta)$ and the temperature $T=T(y,\theta)$ yields

$$u=1-h^2\cos\theta\int_0^y\frac{1-\tilde{y}}{\mu(T(\tilde{y},\theta))}\,\mathrm{d}\tilde{y}, \tag{2.10}$$

$$\psi=hy-h^3\cos\theta\int_0^y\int_0^{\bar{y}}\frac{1-\tilde{y}}{\mu(T(\tilde{y},\theta))}\,\mathrm{d}\tilde{y}\,\mathrm{d}\bar{y}=hy-h^3\cos\theta\int_0^y\frac{(1-\tilde{y})(y-\tilde{y})}{\mu(T(\tilde{y},\theta))}\,\mathrm{d}\tilde{y}, \tag{2.11}$$

$$p=h(1-y)\sin\theta \tag{2.12}$$

and

$$T=1-\frac{Bhy}{1+Bh}. \tag{2.13}$$

Hence the volume flux $Q\ (=\psi(1,\theta))$ is given by

$$Q=h\int_0^1 u\,\mathrm{d}y=h-h^3\cos\theta\int_0^1\int_0^y\frac{1-\tilde{y}}{\mu(T(\tilde{y},\theta))}\,\mathrm{d}\tilde{y}\,\mathrm{d}y, \tag{2.14}$$

which may be re-written as

$$Q=h-\frac{h^3\cos\theta}{3}f, \tag{2.15}$$

[†] Note that the rescaled stream function $\psi=\psi(y,\theta)$ satisfies $u=\frac{1}{h}\frac{\partial\psi}{\partial y}$ and $v=-\frac{\partial\psi}{\partial\theta}+\frac{y}{h}\frac{\mathrm{d}h}{\mathrm{d}\theta}\frac{\partial\psi}{\partial y}$. Leslie, Wilson and Duffy (**27**) erroneously omitted the second term from their corresponding expression for v. Fortunately, none of their subsequent results are affected by this oversight.

where $f = f(\theta)$ (> 0) denotes the fluidity of the fluid film, defined by

$$f = 3\int_0^1 \int_0^y \frac{1-\tilde{y}}{\mu(T(\tilde{y},\theta))}\,\mathrm{d}\tilde{y}\,\mathrm{d}y = 3\int_0^1 \frac{(1-y)^2}{\mu(T(y,\theta))}\,\mathrm{d}y. \tag{2.16}$$

In the special case of constant viscosity $\mu \equiv 1$ the fluidity is simply equal to unity, i.e. $f \equiv 1$.

In the present work we shall be concerned only with "full-film" solutions, i.e. solutions for which h is continuous, finite and non-zero for all $-\pi < \theta \leq \pi$, corresponding to a continuous film of fluid covering the entire outside or inside of the cylinder. In particular, for such solutions equations (2.13) and (2.16) show that f depends on θ only through its dependence on h, and hence, using (2.15), only through its dependence on $\cos\theta$. Hence h, u and T depend on θ only through $\cos\theta$, and so the flow has top-to-bottom symmetry (but not left-to-right symmetry). Moreover, at the top and the bottom of the cylinder ($\theta = \pm\pi/2$) the film thickness is simply $h = Q$ (from which we trivially deduce that $Q > 0$) and the velocity is a uniform (i.e. independent of y) "plug flow" $u \equiv 1$ across the film.

The fluid load in/on the cylinder, M (> 0), is given by

$$M = \int_{-\pi}^{\pi} h\,\mathrm{d}\theta = 2\int_0^{\pi} h\,\mathrm{d}\theta. \tag{2.17}$$

With the viscosity model $\mu = \mu(T)$ prescribed, the film thickness h is determined in terms of Q by the algebraic equation (2.15) in which f is given by (2.16). The value of Q is determined from either an appropriate criticality condition (given in Section 5) or from the condition of prescribed load using (2.17). The properties and behaviour of the solutions in these two cases are discussed in detail in Sections 5 and 6, respectively, but in both cases, the solutions for u, ψ, p and T are given explicitly by (2.10)–(2.13), respectively.

3. The Special Case of Constant Viscosity

If either there is no heat transfer to or from the atmosphere at the free surface (i.e. in dimensional terms if $\alpha_{\mathrm{th}} = 0$) so that $B = 0$ (in which case the fluid film is isothermal with constant temperature $T \equiv 1$) or the viscosity is independent of temperature (i.e. in dimensional terms if $\lambda = 0$) so that $V = 0$ (in which case the fluid film is non-isothermal with non-constant temperature $T \not\equiv 1$), then the fluid has constant viscosity $\mu \equiv 1$ and fluidity $f \equiv 1$. In either case we recover the classical constant-viscosity solution derived by Moffatt (**28**), denoted by $h = h_0$, $u = u_0$, $\psi = \psi_0$, $Q = Q_0$ and $M = M_0$, where

$$u_0 = 1 - \frac{h_0^2\cos\theta}{2}(2-y)y, \tag{3.1}$$

$$\psi_0 = h_0 y - \frac{h_0^3\cos\theta}{6}(3-y)y^2, \tag{3.2}$$

$$Q_0 = h_0 - \frac{h_0^3\cos\theta}{3} \tag{3.3}$$

and

$$M_0 = 2\int_0^{\pi} h_0\,\mathrm{d}\theta. \tag{3.4}$$

Figure 2 shows contours of the flux Q_0 given by (3.3) in the θ/π–h_0 plane, which, since they are by definition curves on which $Q_0 =$ constant, represent candidate solutions for the free surface $h_0 = h_0(\theta)$. In particular, Figure 2 shows that full-film solutions are possible only for values of Q_0 satisfying $0 < Q_0 \leq Q_{\rm c0}$, where $Q_{\rm c0} = 2/3$ denotes the flux of the critical solution above which full-film solutions are not possible, and that these solutions have loads M_0 satisfying $0 < M_0 \leq M_{\rm c0}$, where $M_{\rm c0}$ denotes the load of the critical solution. A detailed description of the other (i.e. non-full-film) solutions of (3.3) is given by Duffy and Wilson (**10**). When $0 < Q_0 \leq Q_{\rm c0}$ the full-film solution of (3.3) for h_0 may be written explicitly in terms of Q_0 and θ as

$$h_0 = \begin{cases} \dfrac{2}{(\cos\theta)^{1/2}} \cos\left[\dfrac{2\pi}{3} - \dfrac{1}{3}\cos^{-1}\left(-\dfrac{3}{2}Q_0[\cos\theta]^{1/2}\right)\right] & \text{if} \quad |\theta| < \pi/2, \\ Q_0 & \text{if} \quad |\theta| = \pi/2, \\ \dfrac{2}{(-\cos\theta)^{1/2}} \sinh\left[\dfrac{1}{3}\sinh^{-1}\left(\dfrac{3}{2}Q_0[-\cos\theta]^{1/2}\right)\right] & \text{if} \quad \pi/2 < |\theta| \leq \pi, \end{cases} \tag{3.5}$$

and has load M_0 satisfying $0 < M_0 \leq M_{\rm c0}$ given by (3.4). The critical solution, denoted by $h_0 = h_{\rm c0}$, $u_0 = u_{\rm c0}$ and $\psi_0 = \psi_{\rm c0}$, is obtained by substituting $Q_0 = Q_{\rm c0} = 2/3$ into (3.1), (3.2) and (3.5), and from (3.4) has load $M_0 = M_{\rm c0}$, where

$$M_{\rm c0} = 2\int_0^\pi h_{\rm c0}\,{\rm d}\theta \simeq 4.44272. \tag{3.6}$$

As Figure 2 shows, the critical film thickness $h_{\rm c0}$ has a corner at $\theta = 0$ (with corresponding corners in all of the other streamlines $\psi_{\rm c0} =$ constant also at $\theta = 0$) given by $h_{\rm c0} = 1 - H_{\rm c0}|\theta| + O(\theta^2)$, where the magnitude of the slope of the corner, denoted by $H_{\rm c0}$, is given by $H_{\rm c0} = 1/\sqrt{6} \simeq 0.40825$.[†]

4. The General Case of Non-Constant Viscosity

In general, if there is heat transfer to or from the atmosphere at the free surface (i.e. in dimensional terms if $\alpha_{\rm th} > 0$) so that $B > 0$ and the viscosity depends on temperature (i.e. in dimensional terms if $\lambda > 0$) so that $V \neq 0$, then the fluid film is non-isothermal with, in general, non-constant temperature, viscosity and fluidity. In the particular case of the exponential viscosity model (2.5) we have

$$\mu = \exp(-V(T-1)) = \exp\left(\frac{BVhy}{1+Bh}\right) = \exp(\mathcal{V}y), \tag{4.1}$$

where, for brevity, we have introduced the notation $\mathcal{V} = \mathcal{V}(\theta)$ defined by

$$\mathcal{V} = \frac{BVh}{1+Bh}, \tag{4.2}$$

so that (2.10) yields the azimuthal velocity

$$u = 1 - \frac{h^2\cos\theta}{\mathcal{V}^2}\left[\mathcal{V} - 1 + (1-\mathcal{V}(1-y))\exp(-\mathcal{V}y)\right], \tag{4.3}$$

[†] Note that Moffatt (**28**) gave slightly inaccurate values of $M_{\rm c0}$ and $H_{\rm c0}$, corresponding to $M_{\rm c0} = 4.428$ and $H_{\rm c0} = 0.577$ in the present notation.

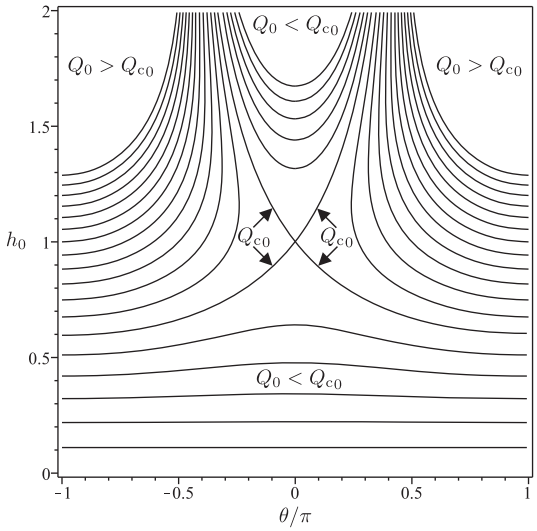

Fig. 2 Contours of the flux in the constant-viscosity case, Q_0, given by (3.3) in the θ/π–h_0 plane. The contours are drawn for $Q_0/Q_{c_0} = 1/6,\ 1/3,\ 1/2,\ \ldots,\ 3$, where $Q_{c_0} = 2/3$.

(2.11) yields the stream function

$$\psi = hy - \frac{h^3\cos\theta}{\mathcal{V}^3}\left[(\mathcal{V}-1)(\mathcal{V}y-1) + 1 - (2-\mathcal{V}(1-y))\exp(-\mathcal{V}y)\right] \tag{4.4}$$

and (2.16) yields the fluidity

$$f = \frac{3}{\mathcal{V}^3}\left[(\mathcal{V}-1)^2 + 1 - 2\exp(-\mathcal{V})\right]. \tag{4.5}$$

Note that the azimuthal velocity profile (4.3) is, in general, very different from the simple parabolic velocity profile in the constant-viscosity case (3.1), and that the fluidity (4.5) is a monotonically decreasing function of $\mathcal{V}$ satisfying $f = O(\exp(-\mathcal{V})/(-\mathcal{V})^3) \to \infty$ as $\mathcal{V} \to -\infty$, $f = 1 + O(\mathcal{V})$ as $\mathcal{V} \to 0$, and $f = O(1/\mathcal{V}) \to 0^+$ as $\mathcal{V} \to \infty$.

Figure 3 shows contours of the flux Q given by (2.15) and (4.5) when $B = 1$ for (a) $V = -5$ and (b) $V = 5$. These plots are typical of those for all values of B and V, and show that, as in the constant-viscosity case, there is a critical flux $Q_c = Q_c(B,V)$ with a corresponding critical load $M_c = M_c(B,V)$ (both of which, of course, now depend on both B and V) such that full-film solutions exist only for $0 < Q \le Q_c$ (i.e. for $0 < M \le M_c$). For future reference, the corresponding critical solution (with $Q = Q_c$ and $M = M_c$) is denoted by $\mu = \mu_c$, $h = h_c$, $u = u_c$, $\psi = \psi_c$, $T = T_c$ and $f = f_c$.

Figure 4 shows streamlines of the flow (drawn for coating flow) when $B = 1$ and $V = 1$ for (a) a prescribed load $M = 4\,(< M_c \simeq 4.73590)$ and (b) the critical case $M = M_c$. In particular, in the case shown in Figure 4 the azimuthal velocity u is always in the same direction as the rotation of the cylinder (i.e. $u \ge 0$ for all $0 \le y \le 1$), and so backflow (i.e. $u < 0$ somewhere in $0 < y \le 1$) does not occur. While this is by far the most common behaviour (i.e. for most values of B and V backflow does not occur), unlike in the special

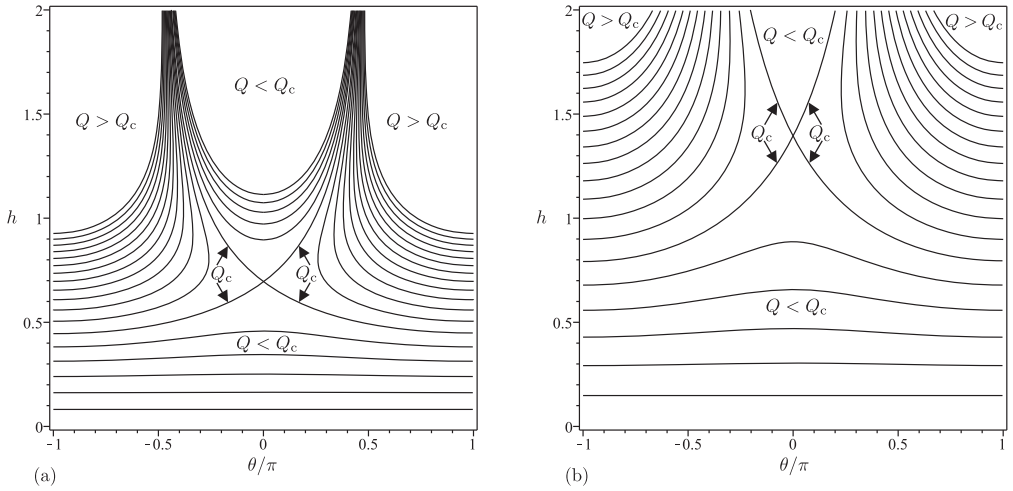

Fig. 3 Contours of the flux in the non-constant-viscosity case, Q, given by (2.15) and (4.5) in the θ/π–h plane when $B = 1$ for (a) $V = -5$ and (b) $V = 5$. The contours are drawn for $Q/Q_c = 1/6$, $1/3$, $1/2$, …, 3, where (a) $Q_c \simeq 0.49107$ and (b) $Q_c \simeq 0.89514$.

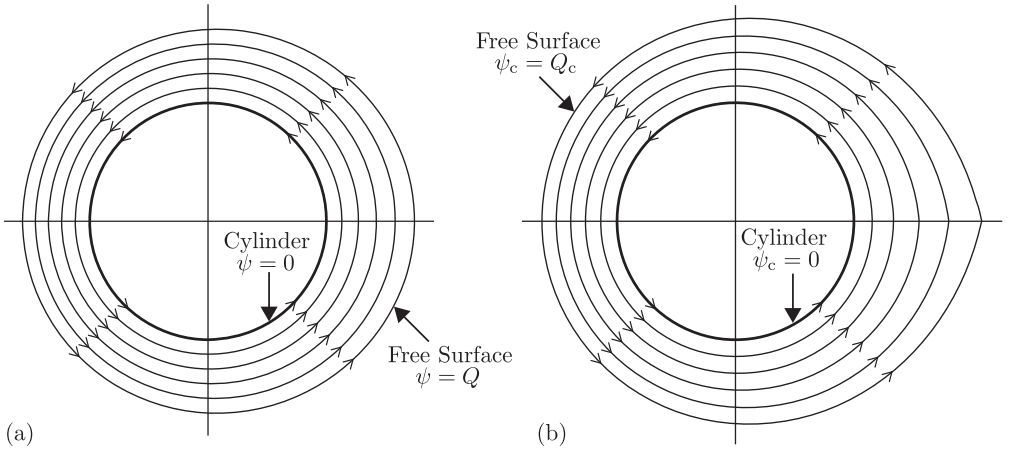

Fig. 4 Streamlines of the flow (drawn for coating flow) plotted for $\psi/Q = 0$ (the cylinder), $1/5$, $2/5$, $3/5$, $4/5$ and 1 (the free surface) when $B = 1$ and $V = 1$ for (a) a prescribed load $M = 4\,(< M_c \simeq 4.73590)$ with $Q \simeq 0.62083\,(< Q_c \simeq 0.70942)$ and (b) the critical case $M = M_c$ with $Q = Q_c$.

case of constant viscosity in which backflow never occurs, in Section 7 we will show that in the general case of non-constant viscosity there is a region of the B–V parameter plane in which backflow occurs in a region on the right-hand side of the cylinder containing the point on the free surface at $\theta = 0$ (i.e. the point $y = 1$ and $\theta = 0$).

5. The Critical Solution

In this Section we consider the properties and behaviour of the non-constant-viscosity critical solution with load $M = M_c$ introduced in Section 4 such that full-film solutions exist only for $0 < M \leq M_c$. Not only is this generalisation of the classical constant-viscosity critical solution of some interest in its own right, but, as we shall see subsequently in Section 6, it is crucial to understanding the properties and behaviour of solutions with a prescribed load.

As Figures 2 and 3 clearly show, the unique feature of the critical solution is that Q has a saddle point at $\theta = 0$ and $h = h_c(0)$, at which point $\partial Q/\partial\theta = 0$ and $\partial Q/\partial h = 0$, which leads to the criticality condition

$$\frac{\mathrm{d}}{\mathrm{d}h}\left(\frac{fh^3}{3}\right) = 1 \tag{5.1}$$

evaluated at $\theta = 0$. For the exponential viscosity model (4.1) the criticality condition (5.1) yields

$$\mathcal{V}^2 + 2\mathcal{V}(V-2) - 2V + 6 - B^2V(V-\mathcal{V})^2 - 2(\mathcal{V}-V+3)\exp(-\mathcal{V}) = 0 \tag{5.2}$$

evaluated at $\theta = 0$, where $\mathcal{V}$ is given by (4.2). Solving (5.2) yields the value of $\mathcal{V}(0)$ and hence the value of $h_c(0)$, and then (2.15) with f_c given by (4.5) yields the value of Q_c and the solution for h_c. The solutions for u_c, ψ_c, T_c and M_c are then given by (4.3), (4.4), (2.13) and (2.17), respectively. As in the constant-viscosity case, the critical film thickness h_c has a corner at $\theta = 0$ (with corresponding corners in all of the other streamlines $\psi_c =$ constant also at $\theta = 0$) given by $h_c = h_c(0) - H_c|\theta| + O(\theta^2)$, where the magnitude of the slope of the corner, denoted by $H_c = H_c(B, V)$ (which, of course, now depends on both B and V) is given by

$$H_c = \left(\frac{V^2\left[(\mathcal{V}-1)^2 + 1 - 2\exp(-\mathcal{V})\right]}{2B^2(V-\mathcal{V})^2[V^2 + 2V(\mathcal{V}-2) - 2\mathcal{V} + 6 - [(V-\mathcal{V}-2)^2+2]\exp(-\mathcal{V})]}\right)^{1/2} \tag{5.3}$$

evaluated at $\theta = 0$. In fact, rather unexpectedly, a general version of (5.3) valid for any viscosity model can be also obtained and is given by

$$H_c = \left[\frac{\displaystyle\int_{\bar{T}}^{1} \frac{(T-\bar{T})^2}{\mu(T)}\mathrm{d}T}{2\displaystyle\int_{\bar{T}}^{1} \frac{T(3T-2\bar{T})}{\mu(T)}\mathrm{d}T \int_{\bar{T}}^{1} \frac{(T-\bar{T})(3T-\bar{T})}{\mu(T)}\mathrm{d}T}\right]^{1/2}, \tag{5.4}$$

where $\bar{T} = T_c(1,0) = 1/(1 + Bh_c(0))$ is the critical free-surface temperature evaluated at $\theta = 0$.

Figure 5 shows the critical film thickness h_c plotted as a function of θ/π for a range of

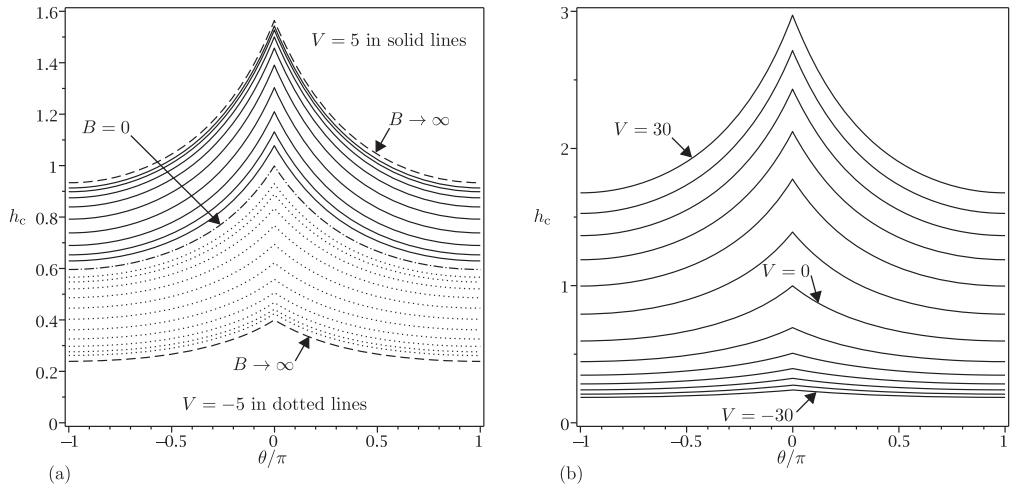

Fig. 5 Critical film thickness h_c plotted as a function of θ/π for (a) $B = 0$ (dash-dot line) and $B = 10^n$ ($n = -1, -0.75, -0.5, \ldots, 1.5$) for $V = -5$ (dotted lines) and $B = 10^n$ ($n = -1, -0.75, -0.5, \ldots, 1$) for $V = 5$ (solid lines) and the leading-order asymptotic solution in the limit $B \to \infty$ for $V = -5$ and $V = 5$ (dashed lines), and (b) $V = -30, -25, -20, \ldots, 30$ for $B = 1$.

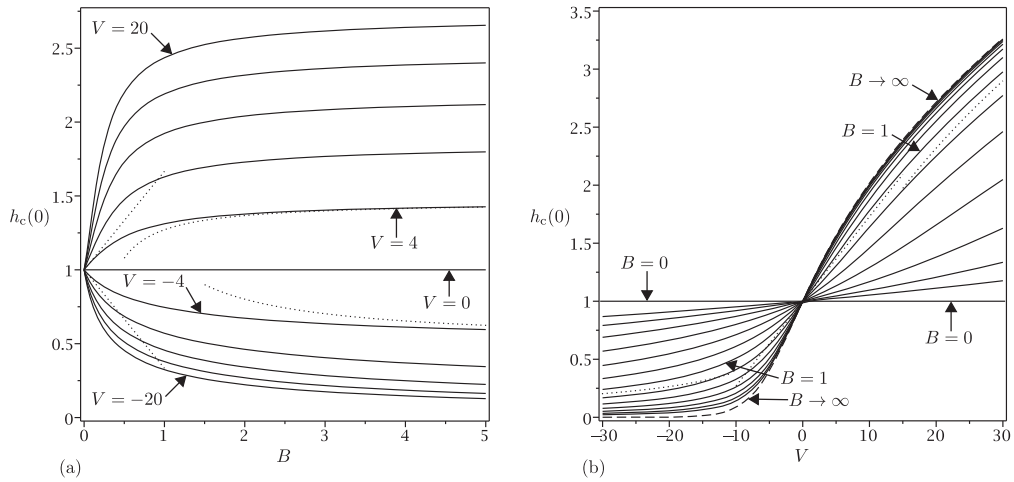

Fig. 6 Critical film thickness at $\theta = 0$, $h_c(0)$, plotted as a function of (a) B for $V = -20, -16, -12, \ldots, 20$ with the asymptotic solutions in the limits $B \to 0^+$ and $B \to \infty$ for $V = -4$ and 4 (dotted lines), and (b) V for $B = 0$ and $B = 10^n$ ($n = -1.5, -1.25, -1, \ldots, 1.5$) with the asymptotic solutions in the limits $V \to 0$, $V \to \infty$ and $V \to -\infty$ for $B = 1$ (dotted lines) and the leading-order asymptotic solution in the limit $B \to \infty$ (dashed line).

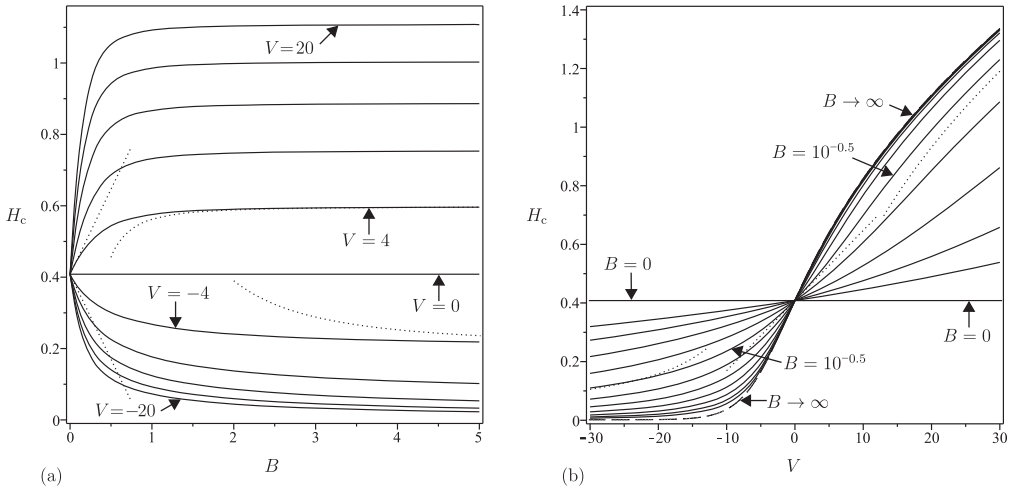

Fig. 7 Magnitude of the slope of the corner in the critical film thickness at $\theta = 0$, H_c, plotted as a function of (a) B for $V = -20, -16, -12, \ldots, 20$ with the asymptotic solutions in the limits $B \to 0^+$ and $B \to \infty$ for $V = -4$ and 4 (dotted lines), and (b) V for $B = 0$ and $B = 10^n$ ($n = -1.5, -1.25, -1, \ldots, 1$) with the asymptotic solutions in the limits $V \to 0$, $V \to \infty$ and $V \to -\infty$ for $B = 10^{-0.5}$ (dotted lines) and the leading-order asymptotic solution in the limit $B \to \infty$ (dashed line).

values of (a) B and (b) V, and Figure 6 shows the critical film thickness at $\theta = 0$, $h_c(0)$, plotted as a function of (a) B for a range of values of V and (b) V for a range of values of B. In particular, Figures 5 and 6 show that h_c is a decreasing function of $|\theta|$, an increasing (decreasing) function of B for positive (negative) V, and an increasing function of V. Figures 7 and 8 show the magnitude of the slope of the corner in the critical film thickness at $\theta = 0$, H_c, and the critical load M_c, respectively, plotted as functions of (a) B for a range of values of V and (b) V for a range of values of B. In particular, Figures 7 and 8 show that both H_c and M_c are increasing (decreasing) functions of B for positive (negative) V, and increasing functions of V.

Figure 9 shows critical velocity profiles u_c at various values of θ in the range $0 \le \theta \le \pi$ when $B = 1$ for (a) $V = -5$ and (b) $V = 5$. The corresponding profiles in the range $-\pi < \theta < 0$ follow immediately from the top-to-bottom symmetry of the flow. In particular, Figure 9 shows that u_c is an increasing function of $|\theta|$, a decreasing (increasing) function of y on the right-hand side $0 \le |\theta| < \pi/2$ (the left-hand side $\pi/2 < |\theta| \le \pi$) of the cylinder, and a uniform plug flow $u_c \equiv 1$ at the top and bottom of the cylinder $|\theta| = \pi/2$. Figure 10 shows the critical free-surface velocity at $\theta = 0$, $u_c(1, 0)$, plotted as a function of (a) B for a range of values of V and (b) V for a range of values of B. In particular, Figure 10 shows that $u_c(1, 0)$ is an increasing (decreasing) function of B for positive (negative) V, an increasing function of V for positive V, but a non-monotonic function of V for negative V.

Figure 11 shows the critical free-surface temperature at $\theta = 0$, $T_c(1, 0)$, plotted as a function of (a) B for a range of values of V and (b) V for a range of values of B. In particular, Figure 11 shows that $T_c(1, 0)$ is a decreasing function of both B and V.

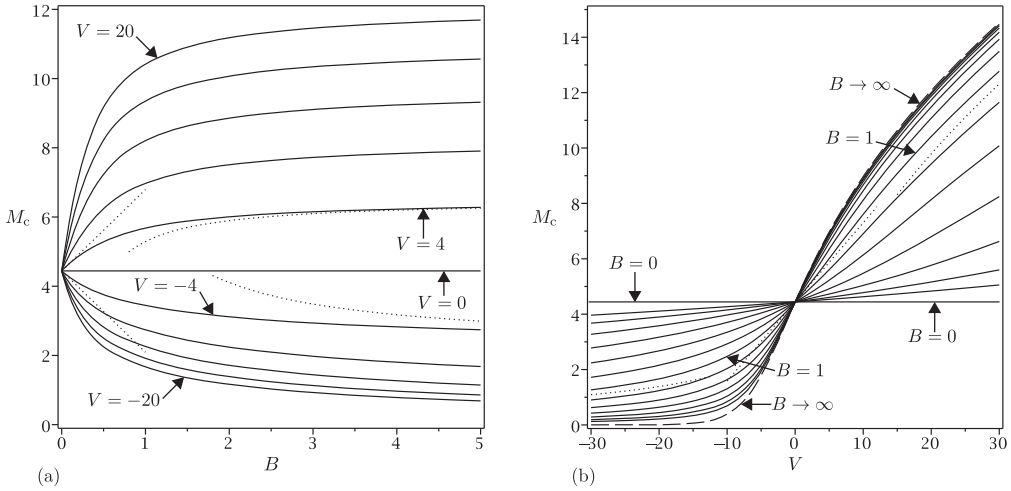

Fig. 8 Critical load M_c plotted as a function of (a) B for $V = -20, -16, -12, \ldots, 20$ with the asymptotic solutions in the limits $B \to 0^+$ and $B \to \infty$ for $V = -4$ and 4 (dotted lines), and (b) V for $B = 0$ and $B = 10^n$ ($n = -1.5, -1.25, -1, \ldots, 1.5$) with the asymptotic solutions in the limits $V \to 0$, $V \to \infty$ and $V \to -\infty$ for $B = 1$ (dotted lines) and the leading-order asymptotic solution in the limit $B \to \infty$ (dashed line).

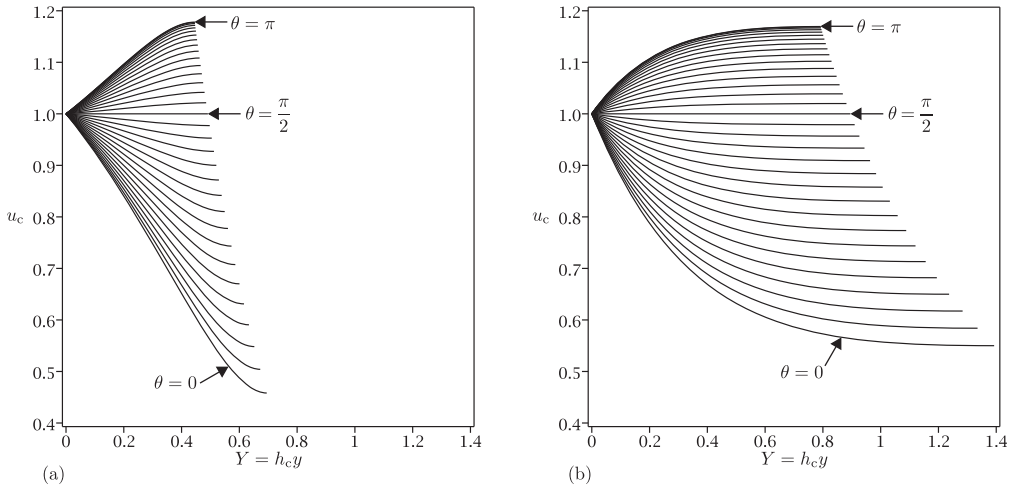

Fig. 9 Critical velocity profiles u_c plotted as a function of $Y = h_c y$ at $\theta = 0, \pi/32, \pi/16, \ldots, \pi$ when $B = 1$ for (a) $V = -5$ and (b) $V = 5$.

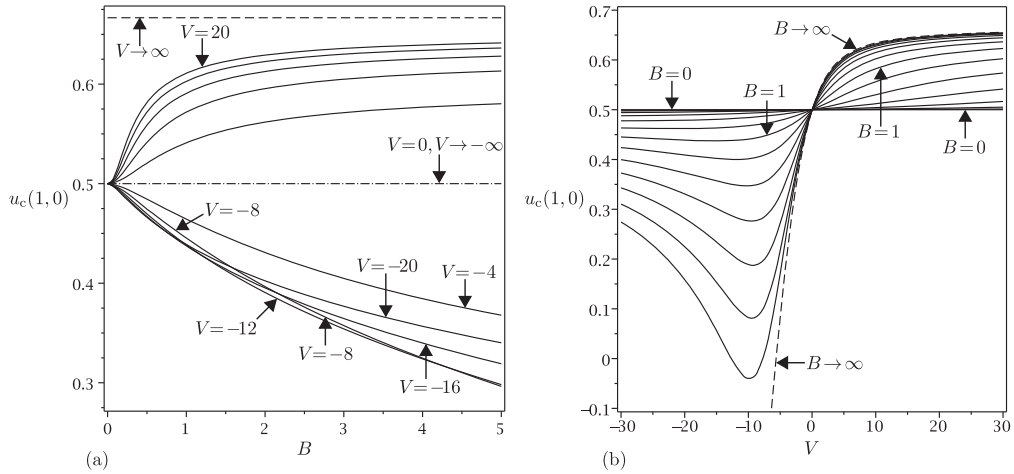

Fig. 10 Critical free-surface velocity at $\theta = 0$, $u_c(1,0)$, plotted as a function of (a) B for $V = -20$, -16, -12, …, 20 with the leading-order asymptotic solution in the limit $V \to \infty$ (i.e. $u_c(1,0) = 2/3$) (dashed line) and the solution for $V = 0$ and the leading-order asymptotic solution in the limit $V \to -\infty$ (i.e. $u_c(1,0) = 1/2$) (dash-dot line), and (b) V for $B = 0$ (i.e. $u_c(1,0) = 1/2$) and $B = 10^n$ ($n = -1.5$, -1.25, -1, …, 1.5) with the leading-order asymptotic solution in the limit $B \to \infty$ (dashed line).

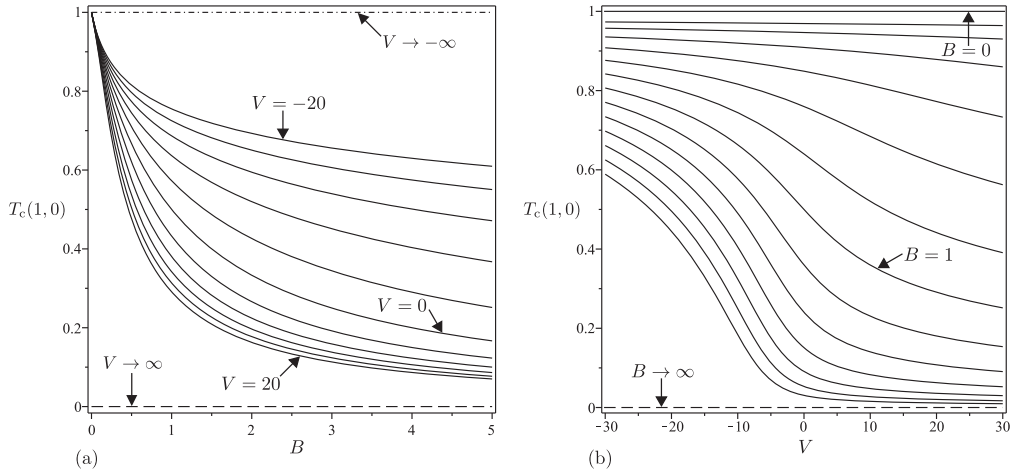

Fig. 11 The critical free-surface temperature at $\theta = 0$, $T_c(1,0)$, plotted as a function of (a) B for $V = -20$, -16, -12, …, 20 with the leading-order asymptotic solution in the limit $V \to \infty$ (i.e. $T_c(1,0) = 0$) (dashed line) and the leading-order asymptotic solution in the limit $V \to -\infty$ (i.e. $T_c(1,0) = 1$) (dash-dot line), and (b) V for $B = 0$ (i.e. $T_c(1,0) = 1$) and $B = 10^n$ ($n = -1.5$, -1.25, -1, …, 1.5) with the leading-order asymptotic solution in the limit $B \to \infty$ (i.e. $T_c(1,0) = 0$) (dashed line).

In order to complete our understanding of the effects of varying B and V on the critical solution, in the following Subsections we analyse the behaviour of the critical solution in the asymptotic limits $B \to 0^+$, $B \to \infty$, $V \to 0$, $V \to \infty$ and $V \to -\infty$.

5.1 *The Limit of Weak Heat Transfer $B \to 0^+$*

At leading order in the limit of weak heat transfer at the free surface, $B \to 0^+$, the free surface is perfectly insulated (i.e. $\partial T_c/\partial y = 0$ on $y = 1$) and the fluid film is isothermal with constant temperature $T_c \equiv 1$, viscosity $\mu_c \equiv 1$ and fluidity $f_c \equiv 1$. Hence the leading-order solutions for h_c, H_c, M_c and u_c are simply the constant-viscosity solutions h_{c0}, H_{c0}, M_{c0} and u_{c0} given in Section 3. The effect of variations in B first appear at $O(B)$, to which order the solutions for h_c, H_c, M_c, u_c and T_c are given by

$$h_c = h_{c0} + \frac{BVh_{c0}}{24}(3h_{c0} + 1) + O(B^2), \tag{5.5}$$

$$H_c = H_{c0} + \frac{7BV}{24\sqrt{6}} + O(B^2), \tag{5.6}$$

$$M_c = M_{c0} + \frac{BV}{24}(3C_{B0} + M_{c0}) + O(B^2), \tag{5.7}$$

$$u_c = u_{c0} - \frac{BVh_{c0}^2 y\cos\theta}{24}\left[h_{c0}(8y^2 - 15y + 6) + 2 - y\right] + O(B^2) \tag{5.8}$$

and

$$T_c = 1 - Bh_{c0}y - \frac{B^2h_{c0}y}{24}\left[V(3h_{c0} + 1) - 24h_{c0}\right] + O(B^3), \tag{5.9}$$

where the constant C_{B0} is given by

$$C_{B0} = 2\int_0^\pi h_{c0}^2\,\mathrm{d}\theta \simeq 3.21962. \tag{5.10}$$

Note that the solutions (5.5)–(5.9) are valid for a general viscosity model satisfying $\mu = 1$ and $\mathrm{d}\mu/\mathrm{d}T = -V$ when $T_c = 1$ to the order shown (but not to higher orders). The same is true for the asymptotic solution in the limit of weak thermoviscosity $V \to 0$ presented subsequently in Subsection 5.3. The solution (5.9) shows that the effect of weak heat transfer at the free surface is to slightly decrease the temperature from its constant isothermal value $T_c \equiv 1$ throughout the fluid film, and thus to slightly increase (decrease) the viscosity from its constant isothermal value $\mu_c \equiv 1$, causing h_c, H_c and M_c to slightly increase (decrease) from their isothermal values when $V > 0$ ($V < 0$). Furthermore, since the sign of the first-order term in (5.8) is simply the sign of $-V\cos\theta$, the effect of weak heat transfer at the free surface is to slightly decrease (increase) u_c from its isothermal value u_{c0} when $V\cos\theta > 0$ ($V\cos\theta < 0$). The asymptotic results (5.5)–(5.7) are included in Figures 6(a), 7(a) and 8(a), respectively.

5.2 *The Limit of Strong Heat Transfer $B \to \infty$*

At leading order in the limit of strong heat transfer at the free surface, $B \to \infty$, the free surface is at the same uniform temperature as the atmosphere (i.e. $T_{\rm c} = 0$ on $y = 1$) and the fluid film has non-constant temperature $T_{\rm c} = \hat{T} = 1 - y$ and viscosity $\mu_{\rm c} = \hat{\mu} = \mu(\hat{T})$. As Duffy and Wilson (**12**) showed, from (2.10) and (2.16) the leading-order solutions for $u_{\rm c}$ and $f_{\rm c}$, denoted by $\hat{u}$ and $\hat{f}$, are given by

$$\hat{u} = 1 - \hat{h}^2 \cos\theta \int_{\hat{T}}^{1} \frac{T}{\mu(T)}\,{\rm d}T \tag{5.11}$$

and

$$\hat{f} = 3\int_{0}^{1} \frac{T^2}{\mu(T)}\,{\rm d}T, \tag{5.12}$$

where $\hat{h}$ denotes the leading-order solution for $h_{\rm c}$. Closed-form expressions for $\hat{f}$ for linear, exponential and Eyring viscosity models are given by Wilson and Duffy (**46**). Moreover, since, for any viscosity model, $\hat{f} = \hat{f}(V)$ is a constant (and not a function of θ as, in general, f is) the leading-order solutions for $h_{\rm c}$, $H_{\rm c}$ and $M_{\rm c}$, denoted by $\hat{h}$, $\hat{H}$ and $\hat{M}$, are given simply by rescaling the corresponding constant-viscosity solutions $h_{\rm c0}$, $H_{\rm c0}$, $Q_{\rm c0}$ and $M_{\rm c0}$ according to $\hat{h} = \hat{f}^{-1/2}h_{\rm c0}$, $\hat{H} = \hat{f}^{-1/2}H_{\rm c0} = (6\hat{f})^{-1/2}$, $\hat{Q} = \hat{f}^{-1/2}Q_{\rm c0}$ and $\hat{M} = \hat{f}^{-1/2}M_{\rm c0}$. For the exponential viscosity model $\mathcal{V} \sim V$ in the limit $B \to \infty$, and so the leading-order solutions for $\mu_{\rm c}$, $u_{\rm c}$, $\psi_{\rm c}$ and $f_{\rm c}$ are given simply by (4.1), (4.3)–(4.5) with $\mathcal{V}$ replaced by V, respectively.

As might have been anticipated, this simple re-scaling property does not extend to higher orders. Specifically, to higher order the solutions for $h_{\rm c}$, $H_{\rm c}$, $M_{\rm c}$ and $T_{\rm c}$ are given by

$$h_{\rm c} = \hat{h} + \frac{3 - (V+3)\hat{f}}{3B\hat{f}} + O\left(\frac{1}{B^2}\right), \tag{5.13}$$

$$H_{\rm c} = \hat{H} + \frac{V^2\hat{f}^2 + 3(V+6)\hat{f} - 18}{3B^2(6\hat{f})^{3/2}} + O\left(\frac{1}{B^3}\right), \tag{5.14}$$

$$M_{\rm c} = \hat{M} + \frac{2\pi[3 - (V+3)\hat{f}]}{3B\hat{f}} + O\left(\frac{1}{B^2}\right) \tag{5.15}$$

and

$$T_{\rm c} = \hat{T} + \frac{\hat{f}^{1/2}y}{Bh_{\rm c0}} - \frac{(3 - V\hat{f})y}{3B^2h_{\rm c0}^2} + O\left(\frac{1}{B^3}\right). \tag{5.16}$$

The solution (5.16) shows that the effect of large-but-finite heat transfer at the free surface is to slightly increase the temperature from its leading-order value $T_{\rm c} = \hat{T} = 1 - y$ throughout the fluid film, and thus to slightly decrease (increase) the viscosity from its leading-order value $\mu_{\rm c} = \hat{\mu} = \exp(Vy)$, causing $h_{\rm c}$, $H_{\rm c}$ and $M_{\rm c}$ to slightly decrease (increase) from their leading-order values when $V > 0$ ($V < 0$). The asymptotic results (5.13)–(5.15) are included in Figures 6(a), 7(a), and 8(a), respectively.

5.3 *The Limit of Weak Thermoviscosity $V \to 0$*

At leading order in the limit of weak thermoviscosity, $V \to 0$, the fluid film has non-constant temperature $T_\mathrm{c} \not\equiv 1$ but constant viscosity $\mu_\mathrm{c} \equiv 1$ and fluidity $f_\mathrm{c} \equiv 1$. Hence, like in the limit $B \to 0^+$, the leading-order solutions for h_c, H_c, M_c and u_c are simply the constant-viscosity solutions $h_{\mathrm{c}0}$, $H_{\mathrm{c}0}$, $M_{\mathrm{c}0}$ and $u_{\mathrm{c}0}$ given in Section 3. The effect of variations in V first appear at $O(V)$, to which order the solutions for h_c, H_c, M_c, u_c and T_c are given by

$$h_\mathrm{c} = h_{\mathrm{c}0} + \frac{BVh_{\mathrm{c}0}[3(1+B)h_{\mathrm{c}0}+1]}{24(1+B)(1+Bh_{\mathrm{c}0})} + O(V^2), \tag{5.17}$$

$$H_\mathrm{c} = H_{\mathrm{c}0} + \frac{BV(3B^2+9B+7)}{24\sqrt{6}(1+B)^3} + O(V^2), \tag{5.18}$$

$$M_\mathrm{c} = M_{\mathrm{c}0} + \frac{BV}{12(1+B)}\int_0^\pi \frac{h_{\mathrm{c}0}[3(1+B)h_{\mathrm{c}0}+1]}{1+Bh_{\mathrm{c}0}}\,\mathrm{d}\theta + O(V^2), \tag{5.19}$$

$$u_\mathrm{c} = u_{\mathrm{c}0} - \frac{BVh_{\mathrm{c}0}^2 y\cos\theta[(1+B)h_{\mathrm{c}0}(8y^2-15y+6)+2-y]}{24(1+B)(1+Bh_{\mathrm{c}0})} + O(V^2) \tag{5.20}$$

and

$$T_\mathrm{c} = 1 - \frac{Bh_{\mathrm{c}0}y}{1+Bh_{\mathrm{c}0}} - \frac{B^2Vh_{\mathrm{c}0}y[3(1+B)h_{\mathrm{c}0}+1]}{24(1+B)(1+Bh_{\mathrm{c}0})^3} + O(V^2). \tag{5.21}$$

The solutions in this limit are somewhat similar to those in the limit $B \to 0^+$ described previously in Subsection 5.1 and have the corresponding physical interpretation. There is, however, one noteworthy difference. Whereas in the limit $B \to 0^+$ the sign of the first-order term in (5.8) is simply the sign of $-V\cos\theta$, in the present limit it is the sign of the somewhat more complicated expression $-V\cos\theta[(1+B)h_{\mathrm{c}0}(8y^2-15y+6)+2-y]$. Thus for $0 < h_{\mathrm{c}0} \leq 1/(1+B)$ and for $0 < y < y_{\mathrm{c}0}$ when $1/(1+B) < h_{\mathrm{c}0} \leq 1$ the effect of weak thermoviscosity is to slightly decrease (increase) u_c from its isothermal value $u_{\mathrm{c}0}$ when $V\cos\theta > 0$ ($V\cos\theta < 0$), whereas for $y_{\mathrm{c}0} < y \leq 1$ when $1/(1+B) < h_{\mathrm{c}0} \leq 1$ the effect is the opposite, where $y = y_{\mathrm{c}0}$ ($0 < y_{\mathrm{c}0} \leq 1$) satisfies $(1+B)h_{\mathrm{c}0}(8y^2-15y+6)+2-y = 0$. This behaviour is the first hint of the occurrence of the backflow described subsequently in Section 7. The asymptotic results (5.17)–(5.19) are included in Figures 6(b), 7(b) and 8(b), respectively.

5.4 *The Limit of Strong Positive Thermoviscosity $V \to \infty$*

In the limit of strong positive thermoviscosity, $V \to \infty$, the solutions for h_c, H_c, M_c, u_c and T_c are given by

$$h_\mathrm{c} = \frac{V^{1/2}h_{\mathrm{c}0}}{\sqrt{3}} - \frac{1}{3B} + O\left(\frac{1}{V^{1/2}}\right), \tag{5.22}$$

$$H_\mathrm{c} = \frac{V^{1/2}}{3\sqrt{2}} + \frac{\sqrt{2}(3B^2-1)}{18B^2V^{1/2}} + O\left(\frac{1}{V}\right), \tag{5.23}$$

$$M_\mathrm{c} = \frac{V^{1/2}M_{\mathrm{c}0}}{\sqrt{3}} - \frac{2\pi}{3B} + O\left(\frac{1}{V^{1/2}}\right), \tag{5.24}$$

$$u_{\rm c} = 1 - \frac{h_{\rm c0}^2 \cos\theta}{3}[1-\exp(-Vy)] - \frac{\sqrt{3}h_{\rm c0}\cos\theta}{9BV^{1/2}}[1-(3Vy+1)\exp(-Vy)] + O\left(\frac{1}{V}\right) \quad (5.25)$$

and

$$T_{\rm c} = 1 - y + \frac{\sqrt{3}y}{BV^{1/2}h_{\rm c0}} - \frac{2y}{B^2 V h_{\rm c0}^2} + O\left(\frac{1}{V^{3/2}}\right). \quad (5.26)$$

These solutions show that at leading order in the limit of strong positive thermoviscosity the temperature is given by $T_{\rm c} = 1-y$ and the viscosity $\mu_{\rm c} = O(\exp(Vy))$ is exponentially large outside a narrow boundary layer of width $O(1/V) \ll 1$ near the cylinder $y = 0$, resulting in a uniform plug flow $u_{\rm c} \equiv 1 - h_{\rm c0}^2\cos\theta/3$ outside the boundary layer and a large film thickness and load of $O(V^{1/2}) \gg 1$. The asymptotic results (5.22)–(5.24) are included in Figures 6(b), 7(b) and 8(b), respectively.

5.5 *The Limit of Strong Negative Thermoviscosity $V \to -\infty$*

In the limit of strong negative thermoviscosity, $V \to -\infty$, the solutions for $h_{\rm c}$, $H_{\rm c}$, $M_{\rm c}$, $u_{\rm c}$ and $T_{\rm c}$ are given by

$$h_{\rm c} = \frac{1}{B(-V)}\left[\log\left(\frac{B^2V^2}{2}\right) - W_{V\infty} - 1\right] + O\left(\frac{\log(-V)^2}{V^2}\right), \quad (5.27)$$

$$H_{\rm c} = \frac{1}{B(-V)} + O\left(\frac{\log(-V)}{V^2}\right), \quad (5.28)$$

$$M_{\rm c} = \frac{1}{B(-V)}\left[2\pi\log\left(\frac{B^2V^2}{2}\right) - C_{V\infty} - 2\pi\right] + O\left(\frac{\log(-V)^2}{V^2}\right), \quad (5.29)$$

$$u_{\rm c} = 1 - \frac{\cos\theta}{B^2V^2}\left[\left(-\frac{B^2V^2W_{V\infty}}{2\cos\theta}\right)^y\left\{\left[\log\left(\frac{B^2V^2}{2}\right) - W_{V\infty}\right](1-y) + y\right\} - \log\left(\frac{B^2V^2}{2}\right) + W_{V\infty}\right] + O\left(\frac{\log(-V)^2}{-V}\right) \quad (5.30)$$

and

$$T_{\rm c} = 1 - \frac{y}{(-V)}\left[\log\left(\frac{B^2V^2}{2}\right) - W_{V\infty} - 1\right] + O\left(\frac{\log(-V)}{V^2}\right), \quad (5.31)$$

where the function $W_{V\infty} = W_{V\infty}(\theta)$ is given by

$$W_{V\infty} = W_0\left(-\frac{\cos\theta}{\rm e}\right) \quad (5.32)$$

and the constant $C_{V\infty}$ is given by

$$C_{V\infty} = 2\int_0^\pi W_{V\infty}\,{\rm d}\theta \simeq -0.73144, \quad (5.33)$$

in which $W_0 = W_0(x)$ denotes the principal real branch of the Lambert W function. Figure 12(a) shows the two real branches of the Lambert W function, which is defined to be the solution for $W = W(x)$ of $W\exp(W) = x$, namely the principal real branch $W_0(x)$

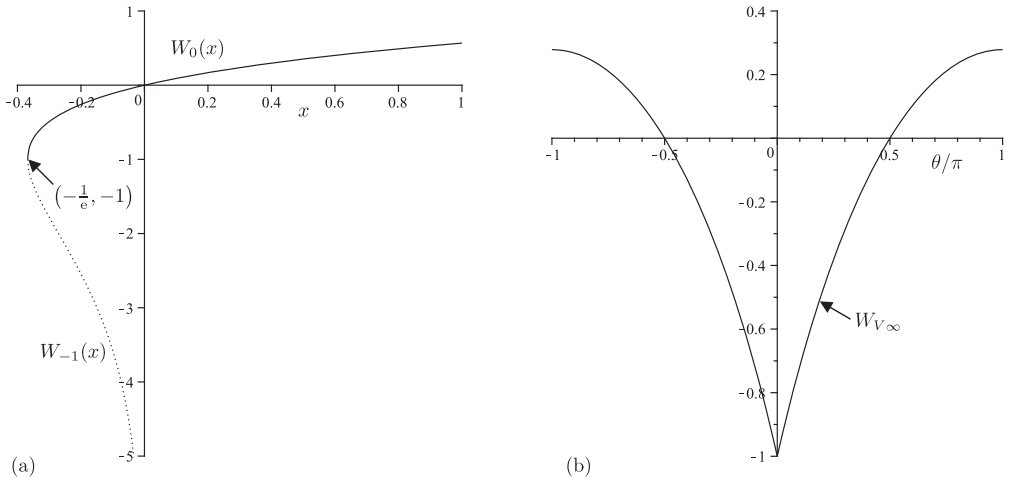

Fig. 12 (a) The two real branches of the Lambert W function, $W_0(x)$ and $W_{-1}(x)$, plotted as functions of x. (b) The function $W_{V\infty} = W_0(-\cos\theta/\mathrm{e})$ plotted as a function of θ/π.

with domain $[-1/\mathrm{e}, \infty)$ and range $[-1, \infty)$ and the lower real branch $W_{-1}(x)$ with domain $[-1/\mathrm{e}, 0)$ and range $(-\infty, -1]$. Figure 12(b) shows the function $W_{V\infty}$ given by (5.32) plotted as a function of θ/π and, in particular, shows that the sign of $W_{V\infty}$ is simply the sign of $-\cos\theta$. The solutions (5.27)–(5.31) show that at leading order in the limit of strong negative thermoviscosity the temperature is given by $T_\mathrm{c} \equiv 1$ and the viscosity $\mu = O(V^{-2y})$ decreases from $O(1)$ at the cylinder $y = 0$ to $O((-V)^{-2}) \ll 1$ at the free surface $y = 1$, resulting in a velocity that increases (decreases) from $u_\mathrm{c} = 1$ at the cylinder [where there is a narrow boundary layer of width $O(1/\log(-V)) \ll 1$] to $u_\mathrm{c} = 1 + W_{V\infty}/2$ at the free surface [where there is another narrow boundary layer also of width $O(1/\log(-V)) \ll 1$] when $\cos\theta < 0$ ($\cos\theta > 0$), and a small film thickness and load of $O(\log(-V)/(-V)) \ll 1$. The asymptotic results (5.27)–(5.29) are included in Figures 6(b), 7(b) and 8(b), respectively.

6. Full-Film Solution with a Prescribed Load

In this Section we consider the properties and behaviour of the non-constant-viscosity full-film solution with a prescribed load M. As described in Section 4, such solutions exist only when $0 < M \leq M_\mathrm{c}$, where M_c is the load of the critical solution described in Section 5 and shown in Figure 8. Thus for a prescribed value of M such solutions exist, in general, only for restricted ranges of values of B and V, and the critical values of B and V for such solutions to exist, denoted by B_c and V_c, are precisely the values of B and V for which the critical solution has load $M_\mathrm{c} = M$. The ranges of values of B and V depend on the relative size of the prescribed load M compared to the load of the critical solution in the limit $B \to 0^+$ (i.e. in the constant-viscosity case), namely $M_{\mathrm{c}0} \simeq 4.44272$, and the load of the critical solution in the limit $B \to \infty$, namely $\hat{M} = \hat{f}^{-1/2} M_{\mathrm{c}0}$, where $\hat{f} = \hat{f}(V)$ is given by (5.12), described previously. Specifically, as Figure 8(a) shows, for positive V there are no full-film solutions for any value of B when $M \geq \hat{M}$, full-film solutions for $B \geq B_\mathrm{c}$ when $M_{\mathrm{c}0} < M < \hat{M}$, and full-film solutions for all values of B when $M \leq M_{\mathrm{c}0}$, while

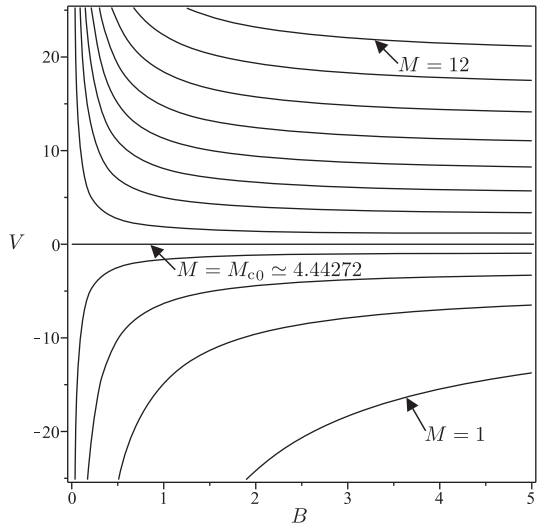

Fig. 13 The critical curves (B_c, V_c) for $M = 1, 2, 3, \ldots, 12$ and $M = M_{c0} \simeq 4.44272$. For each value of M the corresponding curve (B_c, V_c) divides the B–V parameter plane into the region above the curve in which full-film solutions exist and the region below the curve in which they do not exist.

for negative V there are no full-film solutions for any value of B when $M > M_{c0}$, full-film solutions for $B \leq B_c$ when $\hat{M} < M \leq M_{c0}$, and full-film solutions for all values of B when $M \leq \hat{M}$. In particular, if we denote the value of V satisfying $M = \hat{M}$ by $V = V_\infty$, then there are full-film solutions in the limit $B \to \infty$ for $V \geq V_\infty$, but not for $V < V_\infty$. Similarly, as Figure 8(b) shows, for all values of B there are full-film solutions for $V \geq V_c$, but not for $V < V_c$. This behaviour is summarised in Figure 13, which shows the critical curves (B_c, V_c) for a range of values of M. For each value of M the corresponding critical curve (B_c, V_c) divides the B–V parameter plane into the region above the curve in which full-film solutions exist and the region below the curve in which they do not exist.

Figure 14 shows the film thickness h when $M = 2\,(< M_{c0})$ plotted as a function of θ/π for a range of values of B for (a) $V = \pm 4$ and (b) $V = \pm 5$. Figure 14 shows that when $M = 2$ for $V = 5$, $V = 4$ and $V = -4$ (all of which satisfy $V > V_\infty \simeq -4.51567$) there are full-film solutions for all values of B, but for $V = -5 < V_\infty$ there are full-film solutions only for $B \leq B_c \simeq 19.84427$. Figure 15(a) shows the film thickness h plotted as a function of θ/π for a range of values of B when $M = 6\,(> M_{c0})$ and $V = 5$, in which case there are full-film solutions for $B \geq B_c \simeq 0.99344$. Note that there is no corresponding plot for $M = 6\,(> M_{c0})$ and $V = -5$ because there are no full-film solutions when $M > M_{c0}$ and $V < 0$. Figure 15(b) shows the film thickness h plotted as a function of θ/π for a range of values of V when $M = 2\,(< M_{c0})$ and $B = 1$, in which case there are full-film solutions for $V \geq V_c \simeq -14.83331\,(< 0)$. Note that the corresponding plot for $M = 6\,(> M_{c0})$ (which is omitted for brevity) is qualitatively similar to Figure 15(b) except that $V_c > 0$. Figures 14 and 15 also show that h is a decreasing function of $|\theta|$, but, in contrast to the corresponding results for h_c shown in Figure 5, show that near $\theta = 0$ the film thickness h is a decreasing

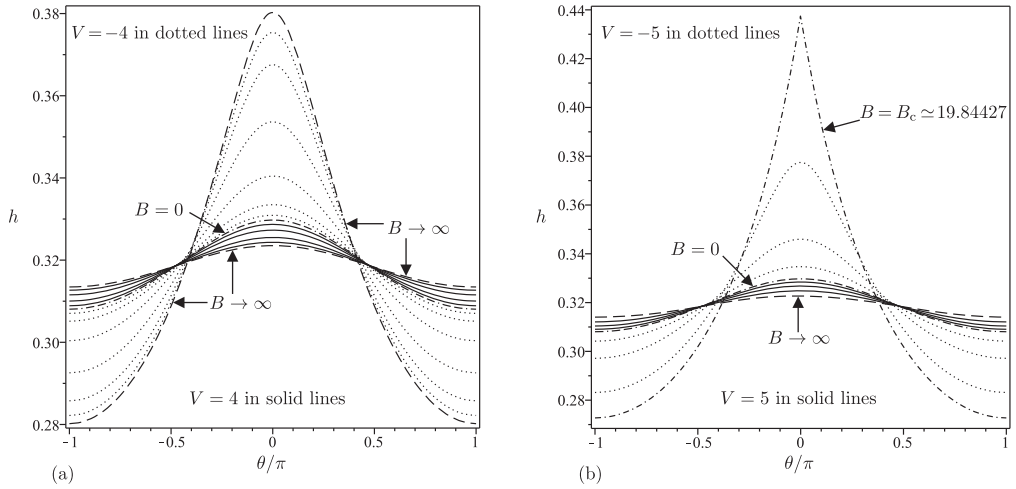

Fig. 14 Film thickness h when $M = 2\,(< M_{\rm c0})$ plotted as a function of θ/π for (a) $B = 0$ (dash-dash-dotted line), $B = 10^n$ ($n = -0.5$, 0, 0.5, 1, 1.5, 2) for $V = -4$ (dotted lines) and $B = 10^n$ ($n = -0.5$, 0, 0.5, 1) for $V = 4$ (solid lines) together with the leading-order asymptotic solution in the limit $B \to \infty$ for $V = -4$ and $V = 4$ (dashed lines), and (b) $B = 0$ (dash-dash-dotted line), $B = 10^n$ ($n = 0$, 0.5, 1) for $V = -5$ (dotted lines) and $B = 10^n$ ($n = -0.5$, 0, 0.5) for $V = 5$ (solid lines) together with the leading-order asymptotic solution in the limit $B \to \infty$ for $V = 5$ (dashed line) and the critical solution for $V = -5$ with $B = B_{\rm c} \simeq 19.84427$ (dash-dotted line).

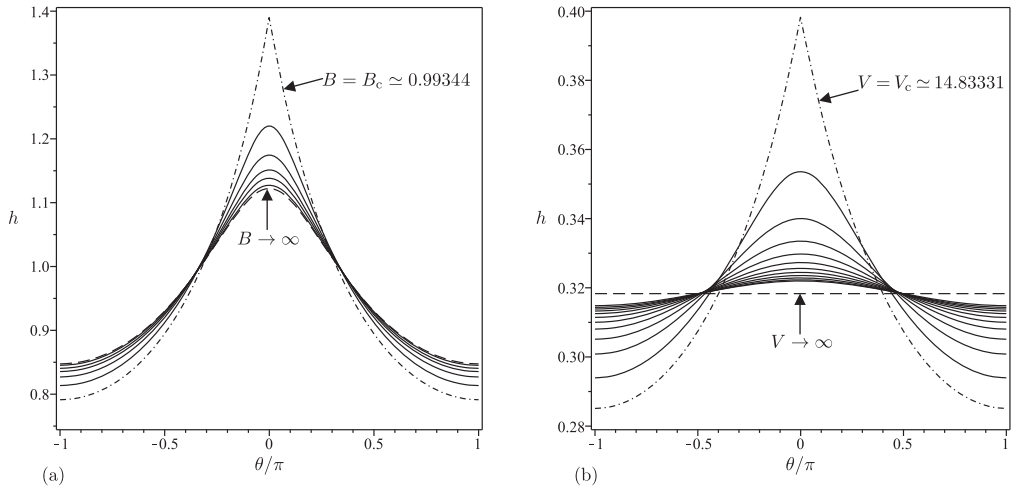

Fig. 15 Film thickness h plotted as a function of θ/π for (a) $B = 10^n$ ($n = 0.25$, 0.5, 0.75, 1, 1.25) (solid lines) together with the leading-order asymptotic solution in the limit $B \to \infty$ (dashed line) and the critical solution with $B = B_{\rm c} \simeq 0.99344$ (dash-dotted line) when $M = 6\,(> M_{\rm c0})$ and $V = 5$, and (b) $V = -12$, -8, -4, ..., 20 (solid lines) together with the leading-order asymptotic solution in the limit $V \to \infty$ (i.e. $h \simeq 0.31831$) (dashed line) and the critical solution with $V = V_{\rm c} \simeq -14.83331$ (dash-dotted line) when $M = 2\,(< M_{\rm c0})$ and $B = 1$.

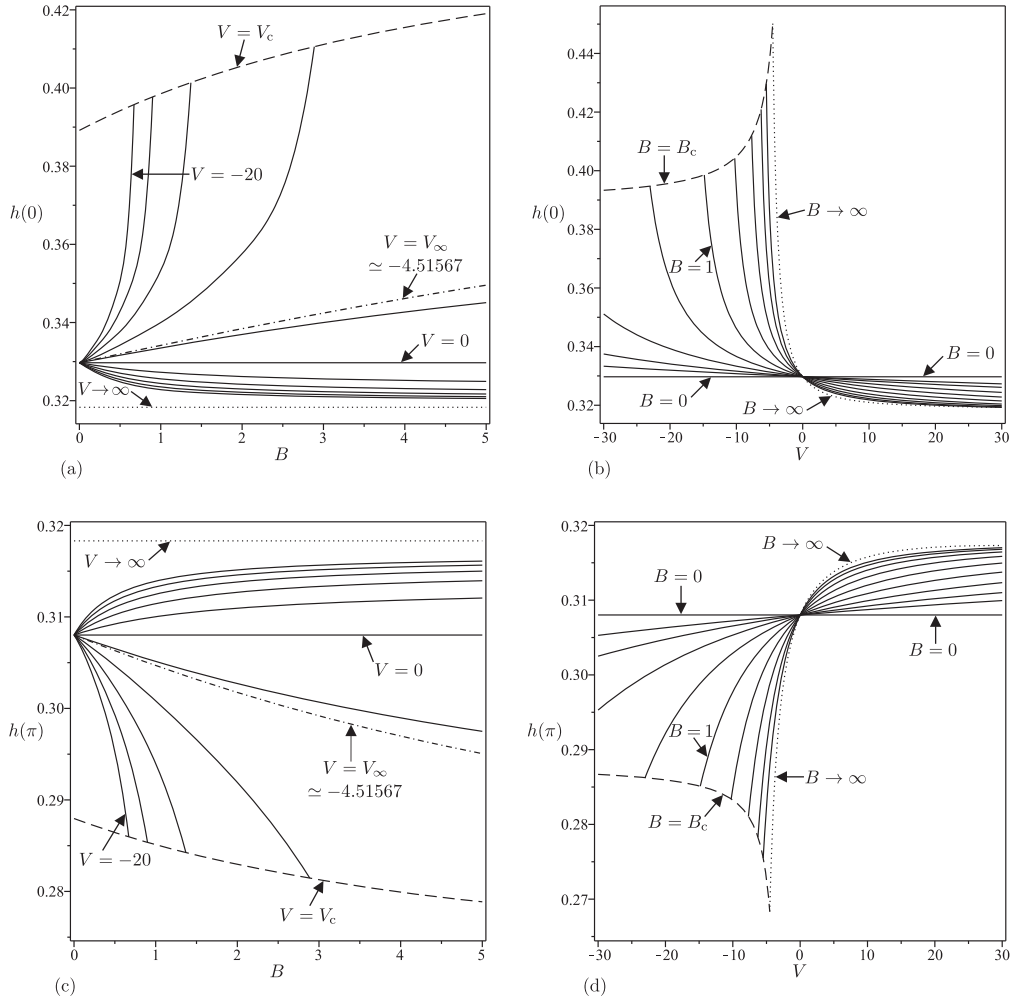

Fig. 16 Film thickness at $\theta = 0$, $h(0)$, and at $\theta = \pi$, $h(\pi)$, when $M = 2\,(< M_{c0})$ plotted as a function of (a,c) B for $V = -20,\ -16,\ -12,\ \ldots,\ 20$ (solid lines) and $V = V_\infty \simeq -4.51567$ (dash-dotted line) together with the leading-order asymptotic solution in the limit $V \to \infty$ (i.e. $h(0) = h(\pi) \simeq 0.31831$) (dotted lines) and the critical solution with $V = V_c$ (dashed line), and (b,d) V for $B = 0$ (i.e. $h(0) \simeq 0.32971$ and $h(\pi) \simeq 0.30802$) and $B = 10^n$ ($n = -1,\ -0.75,\ -0.5,\ \ldots,\ 1$) (solid lines) together with the leading-order asymptotic solution in the limit $B \to \infty$ (dotted line) and the critical solution with $B = B_c$ (dashed line).

(increasing) function of B for positive (negative) V and a decreasing function of V, but that near $\theta = \pi$ it behaves in the opposite way in order to satisfy the condition of prescribed load. Figures 16 and 17 show the film thickness at $\theta = 0$, $h(0)$, and at $\theta = \pi$, $h(\pi)$, plotted as a function of (a,c) B for a range of values of V and (b,d) V for a range of values of B when $M = 2\,(< M_{c0})$ and $M = 6\,(> M_{c0})$, respectively. Note that in Figure 16(a,c) the

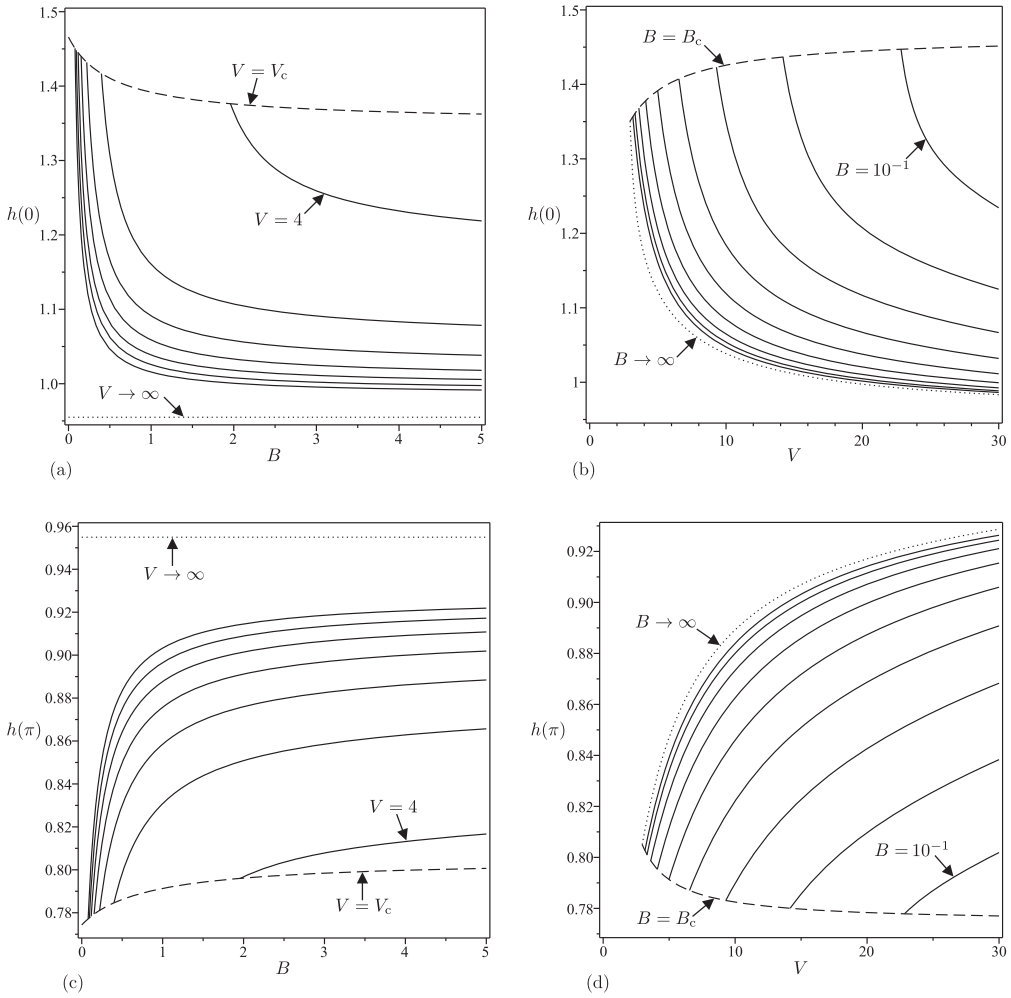

Fig. 17 Film thickness at $\theta = 0$, $h(0)$, and at $\theta = \pi$, $h(\pi)$, when $M = 6\,(> M_{c0})$ plotted as a function of (a,c) B for $V = 4$, 8, 12, ..., 28 (solid lines) together with the leading-order asymptotic solution in the limit $V \to \infty$ (i.e. $h(0) = h(\pi) \simeq 0.95493$) (dotted lines) and the critical solution with $V = V_c$ (dashed line), and (b,d) V for $B = 10^n$ ($n = -1$, -0.75, -0.5, ..., 1) (solid lines) together with the leading-order asymptotic solution in the limit $B \to \infty$ (dotted line) and the critical solution with $B = B_c$ (dashed line).

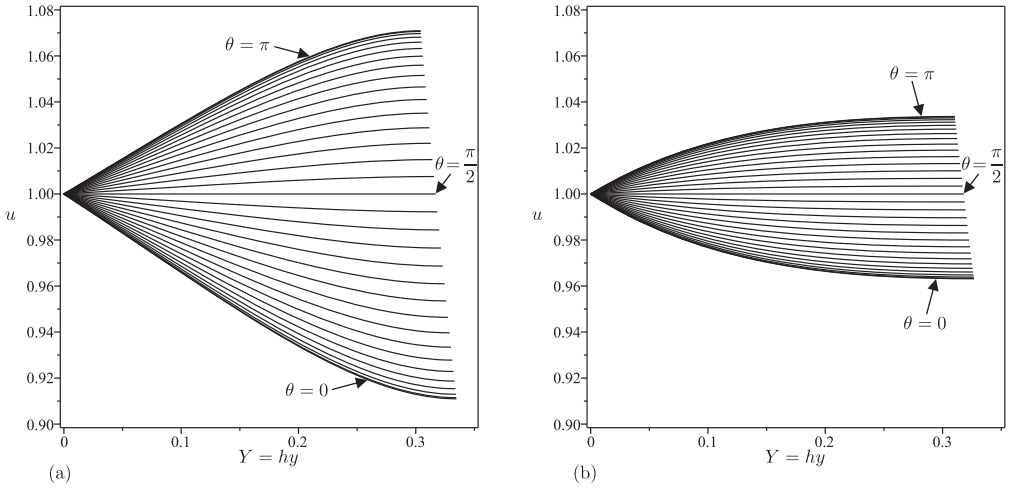

Fig. 18 Velocity profiles u plotted as a function of $Y = hy$ at $\theta = 0$, $\pi/32$, $\pi/16$, $\ldots$, π when $M = 2$ and $B = 1$ for (a) $V = -5$ and (b) $V = 5$.

curve $V = V_\infty \simeq -4.51567$ divides curves that attain the limit $B \to \infty$ from those that terminate at the finite value $B = B_c$ on the curve corresponding to $V = V_c$. In particular, Figures 16 and 17 show that $h(0)$ is a decreasing (increasing) function of B for positive (negative) V and a decreasing function of V, and that $h(\pi)$ behaves in the opposite way.

Figure 18 shows velocity profiles u at various values of θ in the range $0 \leq \theta \leq \pi$ when $M = 2$ and $B = 1$ for (a) $V = -5$ and (b) $V = 5$. Again the corresponding profiles in the range $-\pi < \theta < 0$ follow immediately from the top-to-bottom symmetry of the flow. In particular, Figure 18 shows that the velocity profiles u are qualitatively similar to the critical velocity profiles u_c shown in Figure 9.

Figures 19 and 20 show the free-surface velocity at $\theta = 0$, $u(1,0)$, and at $\theta = \pi$, $u(1,\pi)$, plotted as a function of (a,c) B for a range of values of V and (b,d) V for a range of values of B when $M = 2\,(< M_{c0})$ and $M = 6\,(> M_{c0})$, respectively. In particular, Figures 19 and 20 show that $u(1,0)$ is an increasing (decreasing) function of B for positive (negative) V and an increasing function of V, and that $u(1,\pi)$ behaves in the opposite way.

Figures 21 and 22 show the free-surface temperature at $\theta = 0$, $T(1,0)$, and at $\theta = \pi$, $T(1,\pi)$, plotted as a function of (a,c) B for a range of values of V and (b,d) V for a range of values of B, when $M = 2\,(< M_{c0})$ and $M = 6\,(> M_{c0})$, respectively. In particular, Figures 21 and 22 show that $T(1,0)$ is a decreasing function of B and an increasing function of V, and that $T(1,\pi)$ is also a decreasing function of B but a decreasing function of V.

In the following Subsections we analyse the behaviour of the full-film solution with a prescribed load in the asymptotic limits $B \to 0^+$, $B \to \infty$, $V \to 0$, $V \to \infty$ and $M \to 0$. Note that (unlike in the corresponding analysis of the critical solution described in Subsection 5.5) there is no solution with prescribed load in the limit $V \to -\infty$, and, of course, there is no solution with prescribed load in the limit $M \to \infty$. Moreover, there are solutions with a prescribed load in the limits $B \to 0^+$ and $V \to 0$ only when $M \leq M_{c0}$.

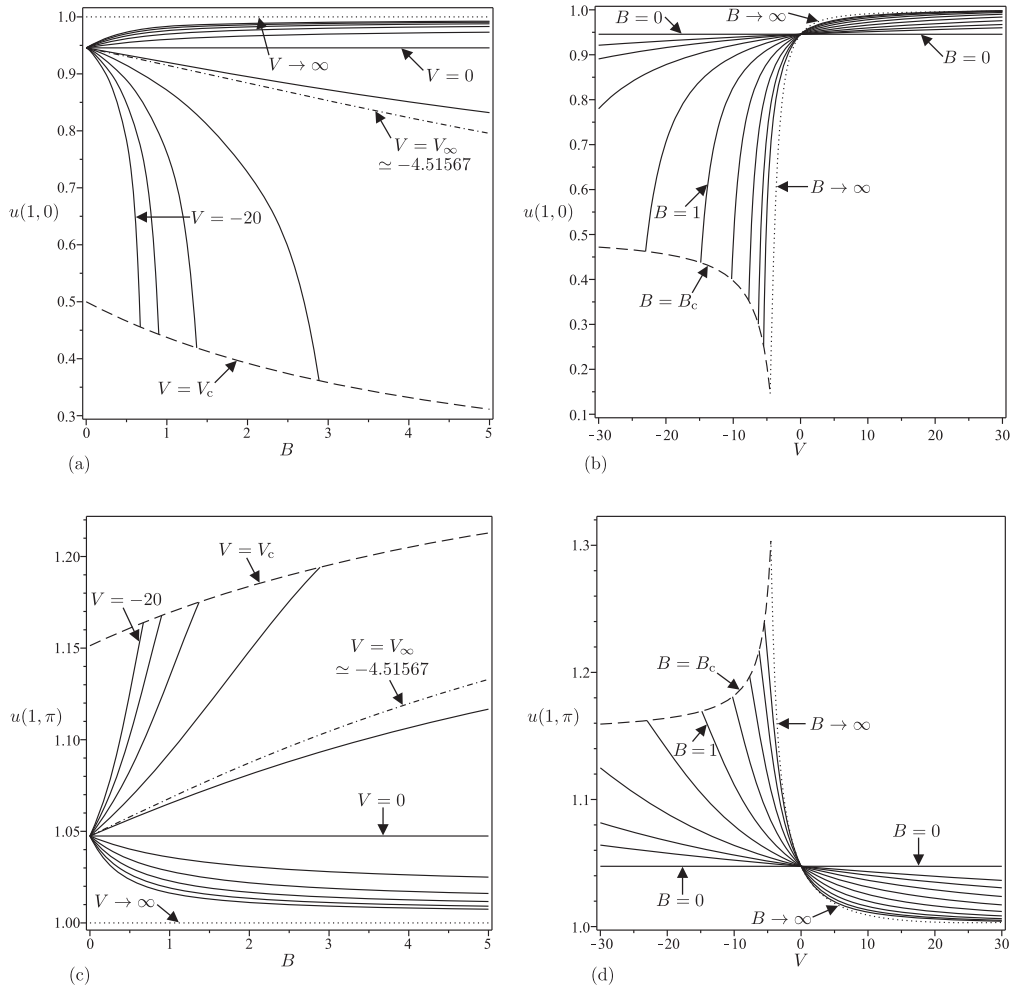

Fig. 19 Free-surface velocity at $\theta = 0$, $u(1,0)$, and at $\theta = \pi$, $u(1,\pi)$, when $M = 2\,(< M_{c0})$ plotted as a function of (a,c) B for $V = -20,\ -16,\ -12,\ \ldots,\ 20$ (solid lines) and $V = V_\infty \simeq -4.51567$ (dash-dotted line) together with the leading-order asymptotic solution in the limit $V \to \infty$ (i.e. $u(1,0) = u(1,\pi) = 1$) (dotted lines) and the critical solution with $V = V_c$ (dashed line), and (b,d) V for $B = 0$ (i.e. $u(1,0) \simeq 0.94565$ and $u(1,\pi) \simeq 1.04744$) and $B = 10^n$ ($n = -1,\ -0.75,\ -0.5,\ \ldots,$ 1) (solid lines) together with the leading-order asymptotic solution in the limit $B \to \infty$ (dotted line) and the critical solution with $B = B_c$ (dashed line).

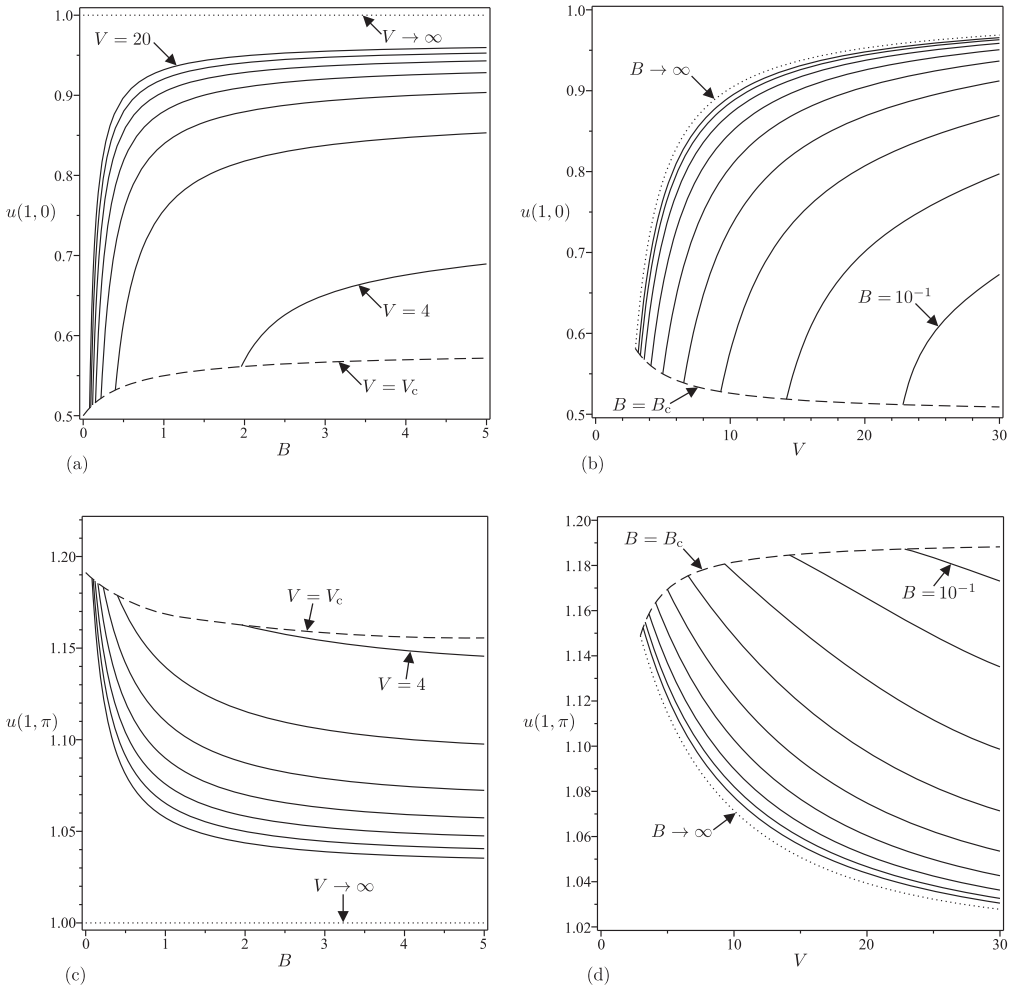

Fig. 20 Free-surface velocity at $\theta = 0$, $u(1,0)$, and at $\theta = \pi$, $u(1,\pi)$, when $M = 6\,(> M_{c0})$ plotted as a function of (a,c) B for $V = 4$, 8, 12, …, 28 (solid lines) together with the leading-order asymptotic solution in the limit $V \to \infty$ (i.e. $u(1,0) = u(1,\pi) = 1$) (dotted lines) and the critical solution with $V = V_c$ (dashed line), and (b,d) V for $B = 10^n$ ($n = -1$, -0.75, -0.5, …, 1) (solid lines) together with the leading-order asymptotic solution in the limit $B \to \infty$ (dotted line) and the critical solution with $B = B_c$ (dashed line).

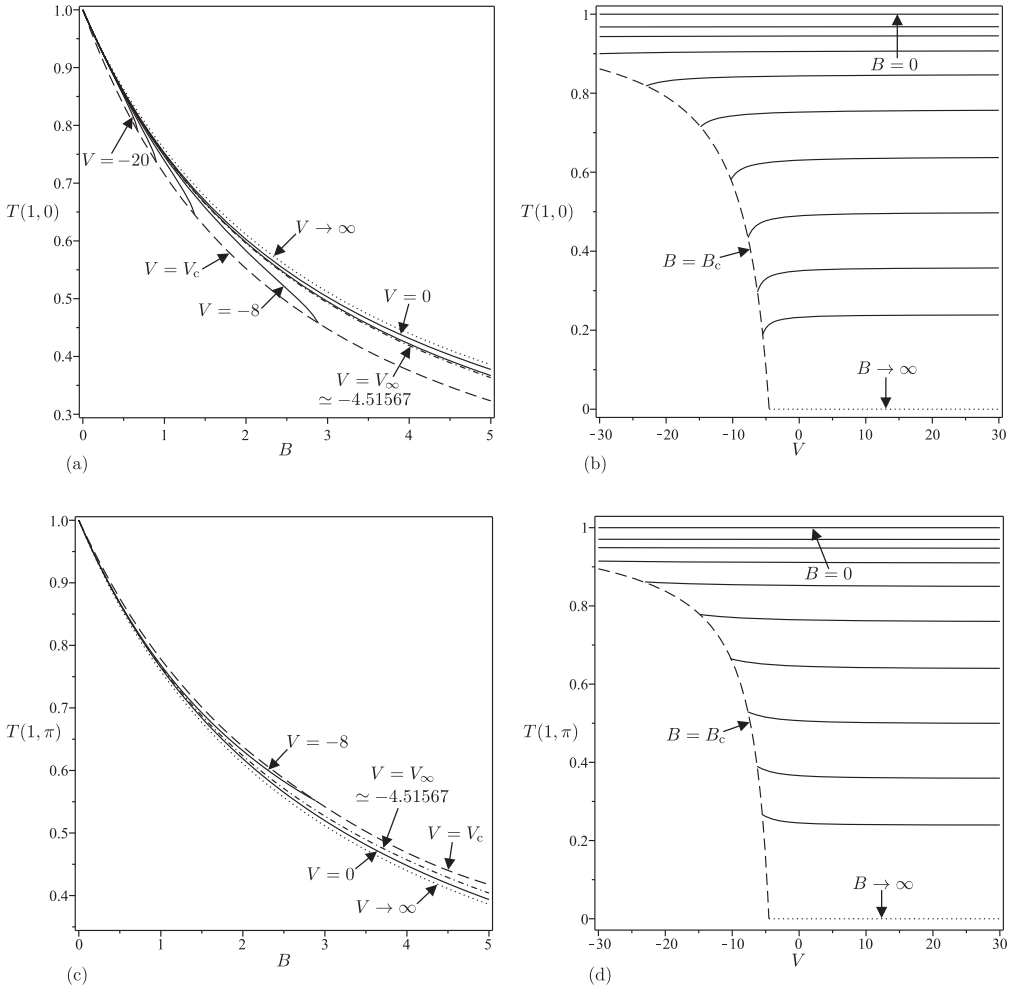

Fig. 21 Free-surface temperature at $\theta = 0$, $T(1,0)$, and at $\theta = \pi$, $T(1,\pi)$, when $M = 2\,(< M_{c0})$ plotted as a function of (a,c) B for $V = -20$, -16, -12, -8, -4, 0 [for clarity, only the curves corresponding to $V = -8$ and $V = 0$ are shown in (c)] (solid lines) and $V = V_\infty \simeq -4.51567$ (dash-dotted line) together with the leading-order asymptotic solution in the limit $V \to \infty$ (dotted line) and the critical solution with $V = V_c$ (dashed line), and (b,d) V for $B = 0$ (i.e. $T(1,0) = T(1,\pi) = 1$) and $B = 10^n$ ($n = -1$, -0.75, -0.5, $\ldots$, 1) (solid lines) together with the leading-order asymptotic solution in the limit $B \to \infty$ (i.e. $T(1,0) = T(1,\pi) = 0$) (dotted lines) and the critical solution with $B = B_c$ (dashed line).

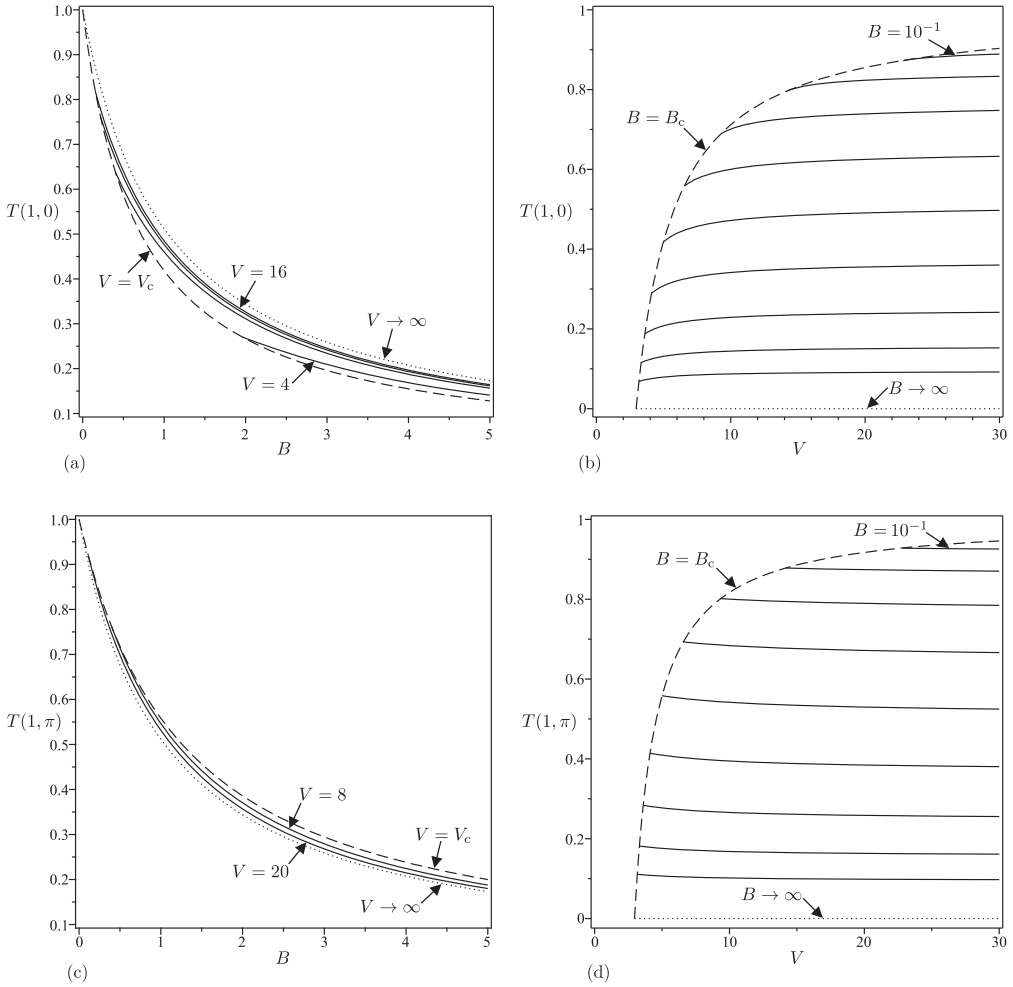

Fig. 22 Free-surface temperature at $\theta = 0$, $T(1,0)$, and at $\theta = \pi$, $T(1,\pi)$, when $M = 6\,(> M_{c0})$ plotted as a function of (a,c) B for $V = 4$, 8, 12, 16 [for clarity, only the curves corresponding to $V = 8$ and $V = 20$ are shown in (c)] (solid lines) together with the leading-order asymptotic solution in the limit $V \to \infty$ (dotted line) and the critical solution with $V = V_c$ (dashed line), and (b,d) V for $B = 10^n$ ($n = -1$, -0.75, -0.5, …, 1) (solid lines) together with the leading-order asymptotic solution in the limit $B \to \infty$ (i.e. $T(1,0) = T(1,\pi) = 0$) (dotted lines) and the critical solution with $B = B_c$ (dashed line).

6.1 *The Limit of Weak Heat Transfer $B \to 0^+$*

In the limit of weak heat transfer at the free surface, $B \to 0^+$, the solutions for h, u and T are given by

$$h = h_0 + \frac{BV(I_{B0} - h_0^4 \cos\theta)}{12(1 - h_0^2 \cos\theta)} + O(B^2), \tag{6.1}$$

$$u = u_0 - \frac{BVh_0 y \cos\theta}{12(1 - h_0^2 \cos\theta)} \left[h_0^2(1 - h_0^2 \cos\theta)(4y^2 - 7y + 2) + (I_{B0} - h_0^2)(2 - y)\right] + O(B^2) \tag{6.2}$$

and

$$T = 1 - Bh_0 y - \frac{B^2 y \left[V(I_{B0} - h_0^4 \cos\theta) - 12h_0^2(1 - h_0^2 \cos\theta)\right]}{12(1 - h_0^2 \cos\theta)} + O(B^3), \tag{6.3}$$

where the constant $I_{B0} = I_{B0}(M_0)$ $(0 < I_{B0} < 1)$ is given by

$$I_{B0} = \frac{\displaystyle\int_0^\pi \frac{h_0^4 \cos\theta}{1 - h_0^2 \cos\theta}\, \mathrm{d}\theta}{\displaystyle\int_0^\pi \frac{1}{1 - h_0^2 \cos\theta}\, \mathrm{d}\theta}, \tag{6.4}$$

and h_0 and u_0 are the constant-viscosity solutions with load $M_0 = M\,(\leq M_{c0})$ given in Section 3. Note that the solutions (6.1)–(6.3) are valid for a general viscosity model satisfying $\mu = 1$ and $\mathrm{d}\mu/\mathrm{d}T = -V$ when $T = 1$ to the order shown (but not to higher orders). The same is true for the asymptotic solution in the limit of weak thermoviscosity $V \to 0$ presented subsequently in Subsection 6.3. Like the corresponding behaviour of the critical solution described in Subsection 5.1, the solution (6.3) shows that the effect of weak heat transfer at the free surface is to slightly decrease the temperature from its constant isothermal value $T \equiv 1$ throughout the fluid film, and thus to slightly increase (decrease) the viscosity from its constant isothermal value $\mu \equiv 1$ when $V > 0$ $(V < 0)$. However, unlike the corresponding behaviour of the critical solution, the effect on h depends on the sign of $V(I_{B0} - h_0^4 \cos\theta)$ (rather than just V). Thus when $V > 0$ $(V < 0)$ the effect of weak heat transfer at the free surface is to slightly decrease (increase) h from its isothermal value when $|\theta| < \bar{\theta}$ with the opposite behaviour when $|\theta| > \bar{\theta}$, where $\theta = \bar{\theta}$ $(0 < \bar{\theta} \leq \pi/2)$ satisfies $I_{B0} - h_0^4 \cos\theta = 0$.

6.2 *The Limit of Strong Heat Transfer $B \to \infty$*

In the limit of strong heat transfer at the free surface, $B \to \infty$, the solutions for h, u and T are given by

$$h = \hat{h} + \frac{h_1}{B} + O\left(\frac{1}{B^2}\right), \tag{6.5}$$

$$u = \hat{u} + \frac{h_0 \cos\theta}{V^2 B \hat{f}^{1/2}} \left[\{V(1 - y) - 2(1 + h_1)\}\, Vy \exp(-Vy) - \{V(1 + 2h_1) - 2(1 + h_1)\}\,(1 - \exp(-Vy))\right] + O\left(\frac{1}{B^2}\right) \tag{6.6}$$

and

$$T = \hat{T} + \frac{\hat{f}^{1/2} y}{B h_0} - \frac{\hat{f}(1+h_1)y}{B^2 h_0^2} + O\left(\frac{1}{B^3}\right), \tag{6.7}$$

where $h_1 = h_1(\theta)$ is given by

$$h_1 = \frac{(I_{B\infty} - h_0^2 \cos\theta)[3 - (V+3)\hat{f}]}{3\hat{f}(1 - h_0^2 \cos\theta)} \tag{6.8}$$

and the constant $I_{B\infty} = I_{B\infty}(M_0)$ $(0 < I_{B\infty} < 1)$ is given by

$$I_{B\infty} = 1 - \pi \left(\int_0^\pi \frac{1}{1 - h_0^2 \cos\theta} \, d\theta \right)^{-1}. \tag{6.9}$$

As in the corresponding analysis of the critical solution described in Subsection 5.2, the leading-order solutions for h and Q, denoted by $\hat{h}$ and $\hat{Q}$, are given simply by rescaling the corresponding constant-viscosity solutions h_0 and Q_0 according to $\hat{h} = \hat{f}^{-1/2} h_0$ and $\hat{Q} = \hat{f}^{-1/2} Q_0$, where $M = \hat{f}^{-1/2} M_0$, and the leading-order solutions for u and f, denoted by $\hat{u}$ and $\hat{f}$, are again given by (5.11) and (5.12), respectively. Like the corresponding behaviour of the critical solution described in Subsection 5.2, the solution (6.7) shows that the effect of large-but-finite heat transfer at the free surface is to slightly increase the temperature from its leading-order value $T = \hat{T} = 1 - y$ throughout the fluid film, and thus to slightly decrease (increase) the viscosity from its leading-order value $\mu = \hat{\mu} = \exp(Vy)$ when $V > 0$ $(V < 0)$. However, unlike the corresponding behaviour of the critical solution, the effect on h depends on the sign of $(I_{B\infty} - h_0^2 \cos\theta)[3 - (V+3)\hat{f}]$ (rather than just $3 - (V+3)\hat{f}$). Thus when $V > 0$ $(V < 0)$, the effect of large-but-finite heat transfer at the free surface is to slightly increase (decrease) h from its isothermal value when $|\theta| < \bar{\theta}$ with the opposite behaviour when $|\theta| > \bar{\theta}$, where $\theta = \bar{\theta}$ $(0 < \bar{\theta} \leq \pi/2)$ satisfies $I_{B\infty} - h_0^2 \cos\theta = 0$.

6.3 *The Limit of Weak Thermoviscosity* $V \to 0$

In the limit of weak thermoviscosity, $V \to 0$, the solutions for h, u and T are given by

$$h = h_0 + \frac{BV[I_{V0}(1 + Bh_0) - h_0^4 \cos\theta]}{12(1 - h_0^2 \cos\theta)(1 + Bh_0)} + O(V^2), \tag{6.10}$$

$$u = u_0 - \frac{BV h_0 y \cos\theta}{12(1 - h_0^2 \cos\theta)(1 + Bh_0)} \left\{ h_0^2 (1 - h_0^2 \cos\theta)(4y^2 - 7y + 2) + \left[I_{V0}(1 + Bh_0) - h_0^2 \right](2 - y) \right\} + O(V^2) \tag{6.11}$$

and

$$T = 1 - \frac{Bh_0 y}{1 + Bh_0} - \frac{B^2 V y \left[I_{V0}(1 + Bh_0) - h_0^4 \cos\theta \right]}{12(1 - h_0^2 \cos\theta)(1 + Bh_0)^3} + O(V^2), \tag{6.12}$$

where the constant $I_{V0} = I_{V0}(M_0, B)$ $(0 < I_{V0} < 1)$ is given by

$$I_{V0} = \frac{\displaystyle\int_0^\pi \frac{h_0^4 \cos\theta}{(1 - h_0^2 \cos\theta)(1 + Bh_0)} \, \mathrm{d}\theta}{\displaystyle\int_0^\pi \frac{1}{1 - h_0^2 \cos\theta} \, \mathrm{d}\theta}, \tag{6.13}$$

and h_0 and u_0 are the constant-viscosity solutions with load $M_0 = M\,(\leq M_{c0})$ given in Section 3. Like the corresponding behaviour of the critical solution described in Subsection 5.3, the solutions in this limit are somewhat similar to those in the limit $B \to 0^+$ described previously in Subsection 6.1 and have the corresponding physical interpretation.

6.4 *The Limit of Strong Positive Thermoviscosity* $V \to \infty$

In the limit of strong positive thermoviscosity, $V \to \infty$, the solutions for h, u and T are given by

$$h = \frac{M}{2\pi} + \frac{M^2 \cos\theta(2\pi + BM)}{8\pi^3 BV} + O\left(\frac{1}{V^2}\right), \tag{6.14}$$

$$u = 1 - \frac{M\cos\theta(2\pi + BM)}{4\pi^2 BV}\left[1 - \exp\left(-\frac{BVMy}{2\pi + BM}\right)\right] + O\left(\frac{1}{V^2}\right) \tag{6.15}$$

and

$$T = 1 - \frac{BMy}{2\pi + BM} - \frac{M^2 y\cos\theta}{2\pi(2\pi + BM)V} + O\left(\frac{1}{V^2}\right). \tag{6.16}$$

These solutions show that, like the corresponding behaviour of the critical solution described in Subsection 5.4, at leading order in the limit of strong positive thermoviscosity the temperature is given by $T = 1 - BMy/(2\pi + BM)$ and the viscosity

$$\mu = O\left[\exp\left(\frac{BVMy}{2\pi + BM}\right)\right] \tag{6.17}$$

is exponentially large outside a narrow boundary layer of width $O(1/V) \ll 1$ near the cylinder $y = 0$, resulting in a uniform plug flow $u \equiv 1$ outside the boundary layer. However, unlike the corresponding behaviour of the critical solution, the leading-order film thickness is an $O(1)$ constant, and the effect of large-but-finite positive thermoviscosity is to slightly decrease T from its leading-order value throughout the fluid film, and thus to slightly decrease (increase) u outside the boundary layer and slightly increase (decrease) h, respectively, from their leading-order values when $\cos\theta > 0$ ($\cos\theta < 0$).

6.5 *The Limit of Small Load* $M \to 0$

In the limit of small load, $M \to 0$, the solutions for h, u and T are given by

$$h = \frac{M}{2\pi} + \frac{M^3\cos\theta}{24\pi^3} + O(M^4), \tag{6.18}$$

$$u = 1 - \frac{M^2\cos\theta(2-y)y}{8\pi^2} + \frac{M^3 BV\cos\theta(3-2y)y^2}{48\pi^3} + O(M^4) \tag{6.19}$$

and

$$T = 1 - \frac{MBy}{2\pi} + \frac{M^2B^2y}{4\pi^2} + O(M^3). \tag{6.20}$$

These solutions show that, as might have been anticipated, at leading order in the limit of small load the film is isothermal, $T \equiv 1$, the viscosity is constant, $\mu \equiv 1$, the film thickness is a small $O(M) \ll 1$ constant, and there is a uniform plug flow $u \equiv 1$.

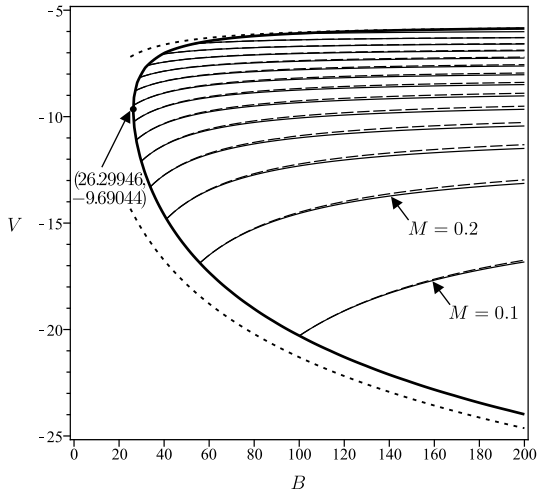

Fig. 23 The regions of the B–V parameter plane in which backflow occurs for $M = 0.1$, 0.2, 0.3, ..., 1.4. For each value of M the region in which backflow occurs is bounded below by the critical curve (B_c, V_c) (solid lines) and above by the curve on which $u(1,0) = 0$ (dashed lines), which meet on the bounding curve on which $u_c(1,0) = 0$ (thick solid line). Also shown are the asymptotic solutions for the upper and lower branches of the bounding curve given by (7.1) and (7.2), respectively, (dashed lines).

7. Backflow

As we noted near the end of Section 4, in the special case of constant viscosity the azimuthal velocity u is always in the same direction as the rotation of the cylinder (i.e. $u \geq 0$ for all $0 \leq y \leq 1$) and so backflow (i.e. $u < 0$ somewhere in $0 < y \leq 1$) never occurs. It is therefore interesting to discover that in the general case of non-constant viscosity there is a region of the B–V parameter plane in which backflow occurs in a region on the right-hand side of the cylinder containing the point on the free surface at $\theta = 0$ (i.e. the point furthest from the cylinder at the azimuthal location at which the local effect of gravity is strongest). Figure 23 shows the regions of the B–V parameter plane in which backflow occurs for a range of values of M. The "bounding" curve corresponding to $u_c(1,0) = 0$ divides the B–V parameter plane into the region to the left of the curve in which $u_c(1,0) > 0$ in which backflow is impossible from the region to the right of the curve in which $u_c(1,0) < 0$ in which backflow is possible (but may or may not actually occur). As we have already seen, for each prescribed value of M full-film solutions exist only above the corresponding critical curve (B_c, V_c) (described in Section 6 and shown in Figure 8). Hence, for sufficiently small prescribed values of M backflow occurs in the narrow region bounded below by the critical curve (B_c, V_c) and above by the curve on which $u(1,0) = 0$, and these curves meet on the bounding curve on which $u_c(1,0) = 0$. In the limit $B \to \infty$ the upper and lower branches of the bounding curve satisfy

$$V = V_{\max} + \frac{2\sqrt{3}V_{\max}(V_{\max}+3)}{B\sqrt{V_{\max}+6}(2V_{\max}+9)} + O\left(\frac{1}{B^2}\right) \tag{7.1}$$

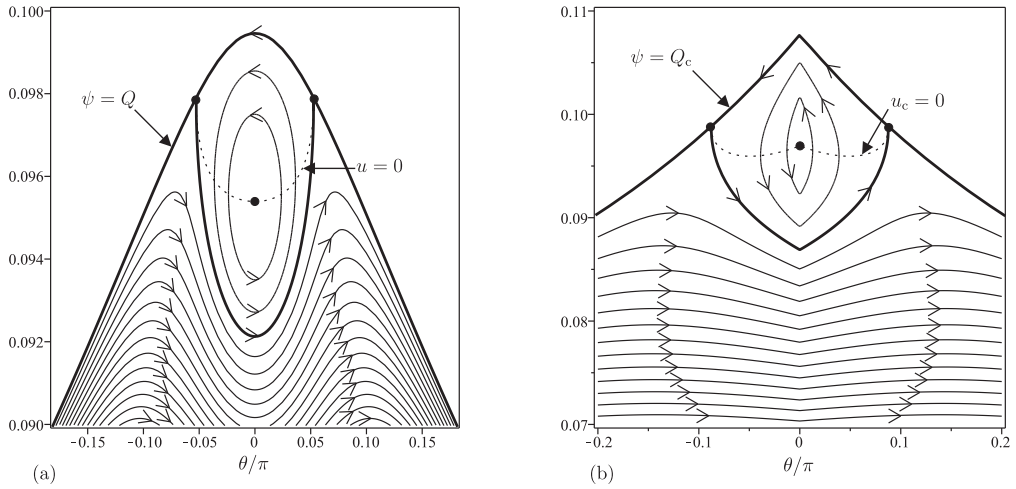

Fig. 24 Details of the streamlines of the flow near $y = 1$ and $\theta = 0$ when $B = 100$ and $V = -10$ for (a) the solution with prescribed load $M = 1/2$ ($Q \simeq 0.07642$) in which the streamlines are drawn for $\psi/Q = 1487/1500$ (the lowest visible streamline), 1488/1500, 1489/1500, ..., 1 (the stagnation streamline), 1501/1500 and 1502/1500 (inside the recirculation region), and (b) the critical solution with load $M = M_c \simeq 0.50800$ ($Q = Q_c \simeq 0.07716$) in which the streamlines are drawn for $\psi/Q = 87/100$ (the lowest visible streamline), 88/100, 89/100, ..., 1 (the stagnation streamline), 101/100 and 102/100 (inside the recirculation region). In both cases the curve on which $u = 0$ is shown with a dashed line and the stagnation points are shown with large dots.

where $V_{\max} \simeq -5.65658$ satisfies $2V_{\max}^2 - 5V_{\max} + 6 - (V_{\max} + 6)\exp(-V_{\max}) = 0$, and

$$V = -4\log B - 4\log(\log B) + 6 - 4\log 2 + O\left(\frac{\log(\log B)}{\log B}\right), \tag{7.2}$$

respectively. In particular, (7.1) and (7.2) show that backflow never occurs for any value of B when $V \geq V_{\max}$, or, equivalently, when $M \geq M_{\max} = \hat{f}(V_{\max})^{-1/2} M_{c0} \simeq 1.50315$. Furthermore, since the bounding curve lies to the right of the point $(26.29946, -9.69044)$, backflow never occurs for any value of V when $B < B_{\min} \simeq 26.29946$.

In order to illustrate backflow, Figure 24 shows details of the streamlines of the flow near $y = 1$ and $\theta = 0$ when $B = 100$ and $V = -10$ in two situations in which backflow occurs. Specifically, Figure 24(a) shows streamlines of the solution with prescribed load $M = 1/2$, while Figure 24(b) shows streamlines of the critical solution with load $M = M_c \simeq 0.50800$.

8. Conclusions

In the present work we obtained a comprehensive description of steady thermoviscous coating and rimming flow on a uniformly rotating horizontal cylinder. We found that, as in the corresponding isothermal problem studied by Moffatt (**28**), there is a critical solution with a corresponding critical load (which depends, in general, on both the Biot number B and the thermoviscosity number V) above which no full-film solutions exist.

In Section 5 we showed that the critical film thickness, h_c, the magnitude of the slope

of the corner in the critical film thickness at $\theta = 0$, H_c, and the critical load, M_c, are increasing (decreasing) functions of B for positive (negative) V, and increasing functions of V. For a positive (negative) fixed value of V the maximum (minimum) possible critical load is attained in the limit of strong heat transfer at the free surface $B \to \infty$ and is given by $\hat{M} = \hat{f}^{-1/2} M_{c0}$, where $\hat{f} = \hat{f}(V)$ is given by (5.12) and $M_{c0} \simeq 4.44272$ is the critical load in the constant-viscosity case. For a fixed value of B the critical film thickness, and hence the critical load, become small like $O(\log(-V)/(-V)) \ll 1$ in the limit of strong negative thermoviscosity $V \to -\infty$ and become large like $O(V^{1/2}) \gg 1$ in the limit of strong positive thermoviscosity $V \to \infty$.

Full-film solutions with a prescribed load M exist only when $0 < M \leq M_c$, and Figure 13 shows how for each prescribed value of M the corresponding critical curve (B_c, V_c) divides the B–V parameter plane into the region above the curve in which full-film solutions exist from the region below the curve in which they do not exist. In particular, there are no full-film solutions with a prescribed load for any value of B when $M \geq \hat{M}$ for positive V and when $M > M_{c0}$ for negative V. In Section 6 we showed that near $\theta = 0$ the film thickness h is a decreasing (increasing) function of B for positive (negative) V, and a decreasing function of B, but that near $\theta = \pi$ it behaves in the opposite way. For a fixed value of V there are full-film solutions in the limit $B \to \infty$ for $V \geq V_\infty$, but not for $V < V_\infty$, where $V = V_\infty$ satisfies $M = \hat{M}$. For a fixed value of B there is no full-film solution in the limit $V \to -\infty$, while the leading-order film thickness is the $O(1)$ constant $h = M/2\pi$ in the limit $V \to \infty$.

In Section 7 we showed that, while by far the most common behaviour of the azimuthal velocity is that it is always in the same direction as the rotation of the cylinder, for sufficiently small prescribed values of M satisfying $M < M_{\max} \simeq 1.50315$ there is a narrow region of the B–V parameter plane shown in Figure 23 in which backflow occurs in a region on the right-hand side of the cylinder containing the point of the free surface at $\theta = 0$. In particular, backflow never occurs for any value of B when $V \geq V_{\max} \simeq -5.65658$ or for any value of V when $B < B_{\min} \simeq 26.29946$.

Lastly, in Appendix A we considered the distinguished limit of strong thermoviscosity $|V| \to \infty$ and weak heat transfer $B \to 0^+$ with $\hat{V} = BV = O(1)$ in which the variation of temperature across the film is small but the variation of viscosity across the film is still $O(1)$, and found qualitative agreement with but some quantitative differences from the previous results. In particular, unlike in the limit $V \to \infty$ described above, in the limit $\hat{V} \to \infty$ the critical film thickness, and hence the critical load, become large like $O(\hat{V}) \gg 1$.

Acknowledgements

The first author (GAL) gratefully acknowledges the financial support of the United Kingdom Engineering and Physical Sciences Research Council (EPSRC) via a Doctoral Training Account (DTA) research studentship. Part of this work as undertaken while the corresponding author (SKW) was a Visiting Fellow in the Department of Mechanical and Aerospace Engineering, School of Engineering and Applied Science, Princeton University, USA, and it was completed while he was a Visiting Fellow in the Oxford Centre for Collaborative Applied Mathematics (OCCAM), Mathematical Institute, University of Oxford, United Kingdom. This publication was based on work supported in part by Award No KUK-C1-013-04, made by King Abdullah University of Science and Technology (KAUST).

References

1. A. Acrivos and B. Jin, Rimming flows within a rotating horizontal cylinder: asymptotic analysis of the thin-film lubrication equations and stability of their solutions, *J. Eng. Math.* (2004) **50** 99–120.

2. J. Ashmore, A. E. Hosoi and H. A. Stone, The effect of surface tension on rimming flows in a partially filled rotating cylinder, *J. Fluid Mech.* (2003) **479** 65–98.

3. N. J. Balmforth and R. V. Craster, Dynamics of cooling domes of viscoplastic fluid, *J. Fluid Mech.* (2000) **422** 225–248.

4. E. S. Benilov, S. B. G. O'Brien and I. A. Sazonov, A new type of instability: explosive disturbances in a liquid film inside a rotating horizontal cylinder, *J. Fluid Mech.* (2003) **497** 201–224.

5. E. S. Benilov, N. Kopteva and S. B. G. O'Brien, Does surface tension stabilize the liquid films inside a rotating horizontal cylinder?, *Q. J. Mech. Appl. Math.* (2005) **58** 185–200.

6. E. S. Benilov and S. B. G. O'Brien, Inertial instability of a liquid film inside a rotating horizontal cylinder, *Phys. Fluids* (2005) **17** 052106.

7. E. S. Benilov, M. S. Benilov and N. Kopteva, Steady rimming flows with surface tension, *J. Fluid Mech.* (2008) **597** 91–118.

8. D. Bercovici, A theoretical model of cooling viscous gravity currents with temperature-dependent viscosity, *Geophys. Res. Lett.* (1994) 21 1177–1180.

9. P.-J. Chen, Y.-T. Tsai, T.-J Liu and P.-Y. Wu, Low volume fraction rimming flow in a rotating horizontal cylinder, *Phys. Fluids* (2007) **19** 128107.

10. B. R. Duffy and S. K. Wilson, Thin-film and curtain flows on the outside of a rotating horizontal cylinder, *J. Fluid Mech.* (1999) **394** 29–49.

11. B. R. Duffy and S. K. Wilson, A rivulet of perfectly wetting fluid with temperature-dependent viscosity draining down a uniformly heated or cooled slowly varying substrate, *Phys. Fluids* (2003) **15** 3236–3239.

12. B. R. Duffy and S. K. Wilson, Large-Biot-number non-isothermal flow of a thin film on a stationary or rotating cylinder, *Eur. Phys. J. Special Topics* (2009) **166** 147–150.

13. P. L. Evans, L. W. Schwartz and R. V. Roy, Steady and unsteady solutions for coating flow on a rotating horizontal cylinder: Two-dimensional theoretical and numerical modeling, *Phys. Fluids* (2004) **16** 2742–2756.

14. P. L. Evans, L. W. Schwartz and R. V. Roy, Three-dimensional solutions for coating flow on a rotating horizontal cylinder: Theory and experiment, *Phys. Fluids* (2005) **17** 072102.

15. D. Goussis and R. E. Kelly, Effects of viscosity variation on the stability of film flow down heated or cooled inclined surfaces: Long-wavelength analysis, *Phys. Fluids* (1985) **28** 3207–3214

16. D. A. Goussis and R. E. Kelly, Effects of viscosity variation on the stability of a liquid film flow down heated or cooled inclined surfaces: Finite wavelength analysis, *Phys. Fluids* (1987) **30** 974–982.

17. E. B. Hansen and M. A. Kelmanson, Steady, viscous, free-surface flow on a rotating cylinder, *J. Fluid Mech.* (1994) **272** 91–107.

18. E. J. Hinch and M. A. Kelmanson, On the decay and drift of free-surface perturbations in viscous thin-film flow exterior to a rotating cylinder, *Proc. R. Soc. Lond. A* (2003)

459 1193–1213.

19. A. E. Hosoi and L. Mahadevan, Axial instability of a free-surface front in a partially filled horizontal rotating cylinder, *Phys. Fluids* (1999) **11** 97–106.

20. R. Hunt, Numerical solution of the free-surface viscous flow on a horizontal rotating elliptical cylinder, *Num. Meth. Part. Diff. Eqns* (2008) **24** 1094–1114.

21. C.-C. Hwang and C.-I. Weng, Non-linear stability analysis of film flow down a heated or cooled inclined plane with viscosity variation, *Int. J. Heat Mass Transfer* (1988) **31** 1775–1784.

22. B. Jin and A. Acrivos, Rimming flows with an axially varying viscosity, *Phys. Fluids* (2004) **16** 633–640.

23. R. E. Johnson, Steady-state coating flows inside a rotating horizontal cylinder, *J. Fluid Mech.* (1988) **190** 321–342.

24. Y. O. Kabova and V. V. Kuznetsov, Downward flow of a nonisothermal thin liquid film with variable viscosity, *J. Appl. Mech. Tech. Phys.* (2002) **43** 895–901.

25. E. A. Karabut, Two regimes of liquid film flow on a rotating cylinder, *J. Appl. Mech. Tech. Phys.* (2007) **48** 55–64.

26. M. A. Kelmanson, On inertial effects in the Moffatt-Pukhnachov coating-flow problem, *J. Fluid Mech.* (2009) **633** 327–353.

27. G. A. Leslie, S. K. Wilson and B. R. Duffy, Non-isothermal flow of a thin film of fluid with temperature-dependent viscosity on a stationary horizontal cylinder, *Phys. Fluids* (2011) **23** 062101.

28. H. K. Moffatt, Behaviour of a viscous film on the outer surface of a rotating cylinder, *J. Méc.* (1977) **16** 651–673.

29. C. J. Noakes, J. R. King and D. S. Riley, On three-dimensional stability of a uniform, rigidly rotating film on a rotating cylinder, *Q. J. Mech. Appl. Math.* (2005) **58** 229–256.

30. C. J. Noakes, J. R. King and D. S. Riley, On the development of rational approximations incorporating inertial effects in coating and rimming flows: a multiple-scales approach, *Q. J. Mech. Appl. Math.*, (2006) **59** 163–190.

31. S. B. G. O'Brien, A mechanism for linear instability in two-dimensional rimming flow, *Q. Appl. Math.* (2002) **60** 283–299.

32. S. B. G. O'Brien and E. G. Gath, The location of a shock in rimming flow, *Phys. Fluids* (1998) **10** 1040–1042.

33. A. A. Osiptsov, Non-isothermal lava flows over a conical surface, *Fluid Dyn.* (2005) **40** 221–232.

34. R. C. Peterson, P. K. Jimack and M. A. Kelmanson, On the stability of viscous free-surface flow supported by a rotating cylinder, *Proc. R. Soc. Lond. A*, (2001) **457** 1427–1445.

35. K. Pougatch and I. Frigaard, Thin film flow on the inside surface of a horizontally rotating cylinder: Steady state solutions and their stability, *Phys. Fluids* (2011) **23** 022102.

36. V. V. Pukhnachev, Motion of a liquid film on the surface of a rotating cylinder in a gravitational field, *J. Appl. Mech. Tech. Phys.* (1977) **18** 344–351.

37. B. Reisfeld and S. G. Bankoff, Nonlinear stability of a heated thin liquid film with variable viscosity, *Phys. Fluids* (1990) **2** 2066–2067.

38. A. Sansom and J. R. King and D. S. Riley, Degenerate-diffusion models for the spreading

of thin non-isothermal gravity currents, *J. Eng. Math.* (2004) **48** 43–68.
39. R. Selak and G. Lebon, Bénard-Marangoni thermoconvective instability in [the] presence of a temperature-dependent viscosity, *J. Phys. II France* (1993) **3** 1185–1199.
40. S. T. Thoroddsen and L. Mahadevan, Experimental study of coating flows in a partially-filled horizontally rotating cylinder, *Exp. Fluids* (1997) **23** 1–13.
41. M. Tirumkudulu and A. Acrivos, Coating flows within a rotating horizontal cylinder: Lubrication analysis, numerical computations, and experimental measurements, *Phys. Fluids* (2001) **13** 14–19.
42. C. H. Tougher, S. K. Wilson and B. R. Duffy, On the approach to the critical solution in leading order thin-film coating and rimming flow, *Appl. Math. Lett.* (2009) **22** 882–886.
43. R. Usha, R. Ravindran and B. Uma, Dynamics and stability of a thin liquid film on a heated rotating disk film with variable viscosity, *Phys. Fluids* (2005) **17** 102103.
44. M. Villegas-Díaz, H. Power and D. S. Riley, Analytical and numerical studies of the stability of thin-film rimming flow subject to surface shear, *J. Fluid Mech.* (2005) **541** 317–344.
45. S. D. R. Wilson and J. Williams, The flow of a liquid film on the inside of a rotating cylinder, and some related problems, *Phys. Fluids* (1997) **9** 2184–2190.
46. S. K. Wilson and B. R. Duffy, On the gravity-driven draining of a rivulet of fluid with temperature-dependent viscosity down a uniformly heated or cooled substrate, *J. Eng. Math.* (2002) **42** 359–372.
47. S. K. Wilson and B. R. Duffy, Strong temperature-dependent-viscosity effects on a rivulet draining down a uniformly heated or cooled slowly varying substrate, *Phys. Fluids* (2003) **15** 827–840.
48. S. K. Wilson and R. Hunt and B. R. Duffy, On the critical solutions in coating and rimming flow on a uniformly rotating horizontal cylinder, *Q. J. Mech. Appl. Math.* (2002) **55** 357–383.
49. L. Wu, Spin coating of thin liquid films on an axisymmetrically heated disk, *Phys. Fluids* (2006) **18** 063602.
50. M.-C. Wu and C.-C. Hwang, Nonlinear theory of film rupture with viscosity variation, *Int. Comm. Heat Mass Transfer* (1991) **18** 705–713.

APPENDIX A

The Distinguished Limit of Strong Thermoviscosity and Weak Heat Transfer $|V| \to \infty$ *and* $B \to 0^+$ *with* $\hat{V} = BV = O(1)$

In this Appendix we consider the distinguished limit discussed by Wilson and Duffy (**47**) of strong thermoviscosity, $|V| \to \infty$, *and* weak heat transfer at the free surface, $B \to 0^+$, such that $\hat{V} = BV = O(1)$, in which, although the variation in temperature across the fluid film is small, specifically $T = 1 - Bhy + O(B^2)$, thermoviscosity effects still enter the problem at leading order, i.e. the variation in viscosity across the fluid film is still $O(1)$. Note that in this limit the *effective thermoviscosity number*, $\hat{V} = BV$, defined in terms of dimensional quantities by

$$\hat{V} = \frac{\lambda(T_0 - T_\infty)\epsilon a \alpha_{\rm th}}{\mu_0 k_{\rm th}}, \tag{A.1}$$

and not the previously defined thermoviscosity number, V, is the appropriate non-dimensional measure of thermoviscosity effects. In the particular case of the exponential viscosity model (4.1)

in this limit $\mathcal{V} \sim \hat{V}h$ and so the leading-order expressions for μ, u, ψ and f are given simply by (4.1), (4.3)–(4.5) with $\mathcal{V}$ replaced by $\hat{V}h$, respectively.

A.1 *The Critical Solution*

Unlike in the general case considered in Section 5, in the present distinguished limit explicit expressions can be obtained for the critical film thickness at $\theta = 0$, $h_{\rm c}(0)$, the magnitude of the slope of the corner in $h_{\rm c}$ at $\theta = 0$, $H_{\rm c}$, and the critical flux, $Q_{\rm c}$, namely

$$h_{\rm c}(0) = \frac{\hat{V}^2 + 2(W_{\hat{V}} + 1)}{2\hat{V}}, \tag{A.2}$$

$$H_{\rm c} = \left(\frac{\hat{V}^4 + 4\hat{V}^2 W_{\hat{V}} + 4(W_{\hat{V}} + 1)^2}{8\hat{V}(W_{\hat{V}} + 1)} \right)^{1/2} \tag{A.3}$$

and

$$Q_{\rm c} = \frac{\hat{V}^2(\hat{V}^2 + 4) - 4(W_{\hat{V}} + 1)^2}{4\hat{V}^3}, \tag{A.4}$$

where $W_{\hat{V}} = W_{\hat{V}}(\hat{V})$ is given by

$$W_{\hat{V}} = \begin{cases} W_0\left(-\exp\left[-\dfrac{\hat{V}^2}{2} - 1 \right] \right) & \text{if} \quad \hat{V} \geqslant 0, \\ W_{-1}\left(-\exp\left[-\dfrac{\hat{V}^2}{2} - 1 \right] \right) & \text{if} \quad \hat{V} < 0, \end{cases} \tag{A.5}$$

where $W_0(x)$ and $W_{-1}(x)$ are again the principal and lower real branches of the Lambert W function, respectively. Figure A shows the quantities $h_{\rm c}(0)$, $H_{\rm c}$, $Q_{\rm c}$ and $M_{\rm c}$ plotted as functions of $\hat{V}$.

In the limit of weak thermoviscosity, $\hat{V} \to 0$, the solutions for $h_{\rm c}$, $H_{\rm c}$, $M_{\rm c}$ and $u_{\rm c}$ are given by the corresponding results in the limit $B \to 0$ given in Subsection 5.1, namely (5.5)–(5.8), with BV and $O(B^2)$ replaced by $\hat{V}$ and $O(\hat{V}^2)$, respectively, and hence have the same physical interpretation.

In the limit of strong positive thermoviscosity, $\hat{V} \to \infty$, the solutions for $h_{\rm c}$, $H_{\rm c}$, $M_{\rm c}$ and $u_{\rm c}$ are given by

$$h_{\rm c} = \frac{\hat{V}\left[1 - (1 - \cos\theta)^{1/2}\right]}{2\cos\theta} + \frac{1}{\hat{V}} + O\left(\frac{1}{\hat{V}^3}\right), \tag{A.6}$$

$$H_{\rm c} = \frac{\hat{V}}{2\sqrt{2}} + O\left(\frac{1}{\hat{V}^3}\right), \tag{A.7}$$

$$M_{\rm c} = 2\hat{V}\log(1 + \sqrt{2}) + \frac{2\pi}{\hat{V}} + O\left(\frac{1}{\hat{V}^3}\right) \tag{A.8}$$

and

$$u_{\rm c} = 1 - \frac{1}{2}\left[1 - (1 - \cos\theta)^{1/2}\right]\left[1 - \exp\left(-\frac{\hat{V}^2\left[1 - (1 - \cos\theta)^{1/2}\right]y}{2\cos\theta}\right)\right] + O\left(\frac{1}{\hat{V}^2}\right). \tag{A.9}$$

These solutions differ from the corresponding results in the limit $V \to \infty$ given in Subsection 5.4, namely (5.22)–(5.25), but have a qualitatively similar physical interpretation. In particular, these solutions show that at leading order in the limit of strong positive thermoviscosity the viscosity

$$\mu = O\left[\exp\left(\frac{\hat{V}^2\left[1 - (1 - \cos\theta)^{1/2}\right]y}{2\cos\theta}\right)\right] \tag{A.10}$$

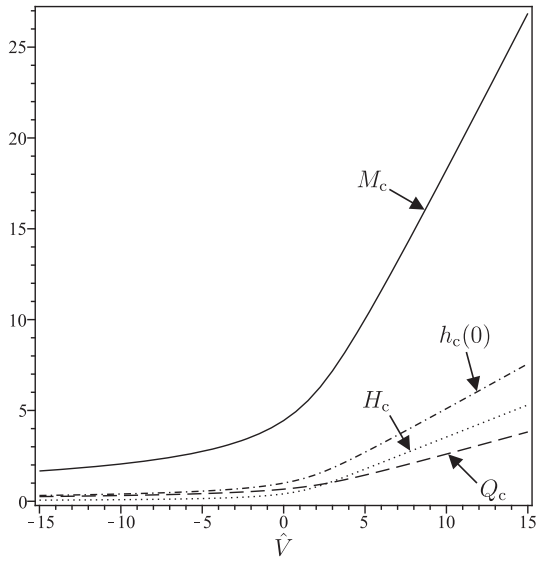

Fig. A The quantities $h_c(0)$ given by (A.2) (dash-dotted line), H_c given by (A.3) (dotted line), Q_c given by (A.4) (dashed line), and M_c (solid line) plotted as functions of $\hat{V}$.

is exponentially large outside a narrow boundary layer of width $O(1/\hat{V}^2) \ll 1$ near the cylinder $y = 0$, resulting in a uniform plug flow $u_c \equiv [1 + (1 - \cos\theta)^{1/2}]/2$ outside the boundary layer and a large film thickness and load of $O(\hat{V}) \gg 1$.

In the limit of strong negative thermoviscosity, $\hat{V} \to -\infty$, the solutions for h_c, H_c, M_c, and u_c are given by

$$h_c = \frac{1}{(-\hat{V})}\left[\log\left(\frac{\hat{V}^2}{2}\right) - W_{V\infty} - 1\right] + O\left(\frac{\log(-\hat{V})^2}{\hat{V}^3}\right), \tag{A.11}$$

$$H_c = \frac{1}{(-\hat{V})} + O\left(\frac{\log(-\hat{V})^2}{\hat{V}^3}\right), \tag{A.12}$$

$$M_c = \frac{1}{(-\hat{V})}\left[2\pi\log\left(\frac{\hat{V}^2}{2}\right) - C_{V\infty} - 2\pi\right] + O\left(\frac{\log(-\hat{V})^2}{(-\hat{V})^3}\right) \tag{A.13}$$

and

$$u_c = 1 - \frac{\cos\theta}{\hat{V}^2}\left[\left(-\frac{\hat{V}^2 W_{V\infty}}{2\cos\theta}\right)^y \left\{\left[\log\left(\frac{\hat{V}^2}{2}\right) - W_{V\infty}\right](1-y) + y\right\} - \log\left(\frac{\hat{V}^2}{2}\right) + W_{V\infty}\right] + O\left(\frac{\log(-\hat{V})^2}{\hat{V}^2}\right), \tag{A.14}$$

where the function $W_{V\infty} = W_{V\infty}(\theta)$ and the constant $C_{V\infty}$ are again given by (5.32) and (5.33), respectively. At leading (but not higher) order these solutions coincide with the corresponding results in the limit $V \to -\infty$ given in Subsection 5.5, namely (5.27)–(5.30), and hence have the same physical interpretation.

A.2 *Full-Film Solution with a Prescribed Load*

In the limit of weak thermoviscosity, $\hat{V} \to 0$, the solutions for h and u are given by the corresponding results in the limit $B \to 0$ given in Subsection 6.1, namely (6.1) and (6.2), with BV and $O(B^2)$ replaced by $\hat{V}$ and $O(\hat{V}^2)$, respectively, and hence have the same physical interpretation.

In the limit of strong positive thermoviscosity, $\hat{V} \to \infty$, the solutions for h and u are given by

$$h = \frac{M}{2\pi} + \frac{M^2 \cos\theta}{4\pi^2 \hat{V}} + O\left(\frac{1}{\hat{V}^2}\right) \tag{A.15}$$

and

$$u = 1 - \frac{M \cos\theta}{2\pi \hat{V}} \left[1 - \exp\left(-\frac{M\hat{V}y}{2\pi}\right)\right] + O\left(\frac{1}{\hat{V}^2}\right). \tag{A.16}$$

These solutions are similar to the corresponding results in the limit $V \to \infty$ given in Subsection 6.4, namely (6.14) and (6.15), from which they can be obtained by writing $V = \hat{V}/B$ and taking the limit $B \to 0$, and hence have the same physical interpretation.

In the limit of small load, $M \to 0$, the solutions for h and u are given by the corresponding results in the limit $M \to 0$ given in Subsection 6.5, namely (6.18) and (6.19), with BV replaced by $\hat{V}$, and hence have the same physical interpretation.

RECENT REPORTS

12/32	Three-dimensional oblique water-entry problems at small deadrise angles	Moore Howison Ockendon Oliver
12/33	Second weak order explicit stabilized methods for stiff stochastic differential equations	Abdulle Vilmart Zygalakis
12/34	The sensitivity of Graphene 'Snap-through' to substrate geometry	Wagner Vella
12/35	The physics of frost heave and ice-lens growth	Peppin Style
12/36	Finite Element Simulation of Dynamic Wetting Flows as an Interface Formation Process	Sprittles Shikhmurzaev
12/37	The Dynamics of Liquid Drops and their Interaction with Solids of Varying Wettabilities	Sprittles Shikhmurzaev
12/38	Dispersal and noise: Various modes of synchrony in ecological oscillators	Bressloff Lai
12/39	Boundary conditions for free surface inlet and outlet problems	Taroni Breward Howell Oliver
12/40	A Branch and Bound Algorithm for the Global Optimization of Hessian Lipschitz Continuous Functions	Fowkes Gould Farmer
12/41	The Orthogonal Gradients Method: a Radial Basis Functions Method for Solving Partial Differential Equations on Arbitrary Surfaces	Piret
12/42	Squeeze-Film Flow in the Presence of a Thin Porous Bed, with Application to the Human Knee Joint	Knox Wilson Duffy McKee
12/43	Gravity-driven draining of a thin rivulet with constant width down a slowly varying substrate	Paterson Wilson Duffy
12/44	The 'Sticky Elastica': Delamination blisters beyond small deformations	Wagner Vella
12/45	Stochastic models of intracellular transport	Bressloff Newby

12/46	The effects of noise on binocular rivalry waves: a stochastic neural field model	Webber Bressloff
12/47	An Ensemble Bayesian Filter for State Estimation	Farmer
12/48	Simulation of cell movement through evolving environment: a fictitious domain approach	Séguis Burrage Erban Kay
12/49	The Mathematics of Liquid Crystals: Analysis, Computation and Applications	Majumdar
12/50	Fourier spectral methods for fractional-in-space reaction-diffusion equations	Bueno-Orovio Kay Burrage
12/51	Meniscal tear film fluid dynamics near Marx's line	Zubkov Breward Gaffney
12/52	Validity of the Cauchy-Born rule applied to discrete cellular-scale models of biological tissues	Davit Osborne Byrne Gavaghan Pitt-Francis
12/53	A thin rivulet or ridge subject to a uniform transverse shear stress at its free surface due to an external airflow	Sullivan Paterson Wilson Duffy
12/54	The Stokes boundary layer for a thixotropic or antithixotropic fluid	McArdle Pritchard Wilson

Copies of these, and any other OCCAM reports can be obtained from:

Oxford Centre for Collaborative Applied Mathematics
Mathematical Institute
24 - 29 St Giles'
Oxford
OX1 3LB
England
www.maths.ox.ac.uk/occam